Spatial variability of liquid water path in marine low cloud: The importance of mesoscale cellular convection.

ROBERT WOOD* and DENNIS. L. HARTMANN

University of Washington, Seattle, Washington

September 26, 2005

Abstract

Liquid water path (LWP) mesoscale spatial variability in marine low cloud over the eastern subtropical oceans is examined using two months of daytime retrievals from the Moderate Resolution Imaging Spectroradiometer (MODIS) on the NASA Terra satellite. Approximately 20000 scenes of size 256×256 km are used in the analysis. It is found that cloud fractional coverage is strongly linked with the (LWP) variability in the cloudy fraction of the scene. We show that in most cases (LWP) spatial variance is dominated by horizonal scales of 10-50 km, and increases as the variance-containing scale increases, indicating the importance of organized mesoscale cellular convection (MCC). A neural network technique is used to classify MODIS scenes by the spatial variability type (no MCC, closed MCC, open MCC, cellular but disorganized). It is shown how the different types tend to occupy distinct geographical regions and different physical regimes within the subtropics, although the results suggest considerable overlap of the large scale meteorological conditions associated with each scene type. We demonstrate that the both the frequency of occurrence, and the variance-containing horizontal scale of the MCC increases as the MBL depth z_i increases. However, for the deepest MBLs, the MCC tends to be replaced by clouds containing cells but lacking organization. In regions where MCC is prevalent, we found a lack of sensitivity of the MCC type (open or closed) to the large scale meteorology, suggesting a mechanism internal to the MBL may be important in determining MCC type. The results indicate that a knowledge of the physics of mesoscale cellular convection (MCC) will be required to completely understand and predict low cloud coverage and variability in the subtropics.

Corresponding author address: Dr. Robert Wood, Atmospheric Sciences, University of Washington, Seattle, WA; *e-mail: robwood@atmos.washington.edu.*

1. Introduction

Low clouds over the oceans are spatially variable on scales from metres to hundreds of kilometres (Cahalan and Snider 1989; Davis et al. 1996; Marshak et al. 1997; Wood and Taylor 2001). This spatial cloud variability needs to be understood because of its importance in cloud-radiation interactions (Cahalan et al. 1994; Barker 1996a,b; Oreopoulos and Davies 1998a,b; Rossow et al. 2002), and in controlling the precipitatation rate (Rotstayn 2000; Pincus and Klein 2000; Larson et al. 2001b; Wood et al. 2002; Stevens et al. 2005).

Parameterizing low cloud cover and spatial variability in large scale numerical models continues to be a challenge. There has been considerable recent focus upon designing cloud schemes that prognose the cloud fraction and internal variability using a saturation deficit probability distribution approach (e.g. Smith 1990; Tompkins 2002). Testing these schemes using observational data has lagged behind their conception. These schemes contain implicit relationships between the distribution moments and the cloud cover that are amenable to examination using observations. Key outstanding questions are what relationships are observed between the cloud fraction and internal cloud variability in cloud liquid water path? Can these relationships be modeled using simple ideas?

It is common for low clouds, most of which occur within the marine boundary layer (MBL), to self-organize into mesoscale cellular convection (MCC) (see reviews by Agee et al. 1973; Atkinson and Zhang 1996), with dominant horizontal scales much greater than the depth of the MBL. Mesoscale cellular convection can exist in the open form (where narrow regions of cloud form around the cell edges with broad regions of clearing between), the closed form (where broad regions of thick stratiform cloud in the cell centers with relatively narrow regions of thinning or clearing at the edges), or as isolated cells with no clear organization. The MCC aspect ratios (cell center separation:MBL depth) reported in field studies are typically 3-40 (Atkinson and Zhang 1996), significantly larger than those (usually 2-4) found in Bénard-Rayleigh convection. MCC is the predominant cloud structure for stratocumulus when the boundary layer is deeper than 1 km (Atkinson and Zhang 1996) and is found less often in very shallow stratus-topped boundary layers. A qualitative climatology of the prevalence of closed and open MCC over the global oceans was introduced by Agee et al. (1973), showing that closed MCC forms preferentially over cold ocean currents and open MCC preferentially over warm ocean currents. Little work has been carried out, however, to quantitatively link cloud cover and spatial variability to the cell types and scales associated with MCC.

In this paper we examine aspects of the mesoscale spatial variability in low clouds over the subtropical eastern oceans, where these clouds are extensive, using satellite data. We use liquid water path derived from visible retrievals as it is directly related to thermodynamic and structural characteristics. Our chief motivation for this work is a desire to quantify the relationships between important cloud characteristics (cloud fraction and moments of the liquid water path distribution), to examine how these vary with mesoscale cellular convection characteristics, and to better understand their associations with the large scale meteorology.

Section 2 describes the data and analysis methodology. In section 3, we examine links between cloud fractional cover and the cloud LWP variability. Section 4 explores links between LWP spatial variability and mesoscale cellular convection. In section 5 we investigate meteorological controls on MCC type and scale. Section 6 presents a discussion and suggestions for future work.

2. Data and methodology

a. *Satellite data and physical parameter estimation*

We use 1 km (at nadir) data from the Moderate Resolution Imaging Spectroradiometer (MODIS) on the NASA Terra sun-synchronous satellite (King et al. 1992). The MODIS cloud product uses visible/near-IR radiances (King et al. 2003) to derive optical thickness τ and near-cloud top effective radius $r_{e,top}$ resolution for cloudy pixels in daytime ($\sim$ 10:30 LST) scenes. Only those pixels within 45° of nadir (i.e. the central 1030 pixels of the scan) are used. The MODIS cloud mask (Ackerman et al. 2002) is used to determine which pixels are cloudy, and therefore the cloud fractional coverage CF. Data from each granule are interpolated onto a 1×1 km across- and along-track grid (1280 km across track, 2030 km along track).

Estimation of liquid water path LWP from the $r_{e,top}$ and τ requires a model of the cloud vertical structure. Often, the cloud is modelled as having constant liquid water content and $r_{e,top}$ in the vertical (e.g. Han et al. 1994) which gives $LWP = \frac{2}{3}\rho_w \tau r_{e,top}$, with ρ_w the density of liquid water. However, observations of boundary layer clouds indicate that the liquid water content is often an approximately linear function of height above cloud base, and that the cloud droplet concentration is approximately constant with height (e.g. Nicholls and Leighton 1986; Brenguier et al. 2000; Wood 2005). This model, used here, results in a relationship $LWP = \frac{5}{9}\rho_w \tau r_{e,top}$, giving LWP values a factor of 5/6=0.8$\dot{3}$ times those using the constant LWC, r_e model. The detection limit for LWP is roughly that corresponding to a visible optical thickness of $\tau = 1$, although some lower values are reported for cloud-classified pixels. We modify the cloud mask to classify as clear pixels with $LWP < 5$ g m^{-2}. This does not have a marked effect upon the derived statistics, but it is important when comparing with analytical models of the LWP probability density function. Based upon the optical thickness error analysis of Pincus et al. (1995), and the error analysis presented in King et al. (1997), a conservative error for the pixel level LWP estimates is roughly 20-40%, although the relative error from pixel to pixel is likely to be considerably less than this.

MBL depth z_i is estimated from the difference between sea surface temperature and cloud top temperature, using vertical structure from the MBL model of Park et al. (2004), as described in Wood and Bretherton (2004). Estimates of the accuracy of this techinique suggest that the uncertainty in each z_i estimate is approximately 200-300 m (Wood and Bretherton 2004).

b. *Scene selection*

Our basic unit of analysis is a "scene", a 256×256 (km)^2 portion of the MODIS swath. Scenes containing only warm cloud are selected using the MODIS thermal IR cloud top temperature (Ma et al. 2000). Only wholly oceanic scenes are analyzed. Some scenes are rejected because of clear instrumental or calibration errors resulting in unphysically large τ. The occurrence of such scenes is uncorrelated with cloud characteristics and so should not bias the results. Scenes are oversampled at increments of 128 km in each direction which gives an approximate restoration of the degrees of freedom lost through data windowing.

Two regions of the East Pacific dominated by low cloud are chosen for this study (see Table 1). All available data from September/October 2000 are used. Figure 1 shows the regions, together with contours that give the fraction of MODIS scenes accepted for analysis. The ISCCP (Rossow and Schiffer 1991) 16 year climatological mid+high cloud amount for September/October (assuming random overlap) is also shown. Over much of the two regions, particularly in the SE Pacific, the mid+high cloud amount is less than 10-15% and the fraction of scenes analysed exceeds 50%, demonstrating the dominance of low cloud, and the lack of high clouds to the east of the subtropical gyres. This fraction decreases both equatorward, due to the presence of clouds associated with deep convection, and towards the midlatitudes, where deep frontal clouds are prevalent. The curious peak in ISCCP mid+high cloud off the coast of southern Peru/northern Chile probably reflects a misdiagnosis of low clouds as midlevel clouds caused by the extremely strong inversions representative of this region.

c. *Example scenes*

To demonstrate the range of observed cloud variability in the subtropical MBL we use four test scenes containing boundary layer cloud types and structures representative of the range found in MBL clouds (Fig. 2). These will be used to demonstrate the analysis methods described below. Scene (a) contains relatively homogeneous stratus without clearly defined mesoscale cellular convection, which is common in near coastal waters in the NE Pacific. Scene (b) contains relatively unbroken stratocumulus cloud with small mesoscale convective cells typical of the extensive stratocumulus sheets over the oceans to the west of continents. Scene (c) contains large stratocumulus cells with breaks typical of the transition regions in the trade wind boundary layer. Scene (d) contains open-celled MCC. Dates and locations, together with a number of parameters (which will be explained below) obtained for each of these scenes are given in Table 2.

d. *Probability density functions, power spectra, lengthscales*

This study is concerned with the spatial variability of LWP and its dependence upon spatial scale. We use (a) probability density functions (pdfs), and (b) power spectral analysis to examine variance as a function of spatial scale.

Probability density functions (pdfs) of LWP for the cloudy pixels in each scene are derived. From these various moments are estimated, and these are used to examine connections between cloud variability and cloud fractional cover. We denote the mean and standard deviation of LWP over the cloudy pixels of the scene as $\overline{LWP}$ and σ_{LWP}. Following Barker (1996b) and Oreopoulos and Davies (1998a) we use $\gamma_{LWP} = (\overline{LWP}/\sigma_{LWP})^2$ as a nondimensional homogeneity parameter. Figure 3 shows a comparison of the LWP pdfs for the four example scenes. A clear shift from a modal to a nonmodal pdf form is seen with decreasing cloud cover. Accompanying this shift is a general decrease in γ_{LWP} as the cloudy fraction of the scene becomes more inhomogeneous, together with an increase in the skewness of the distribution (Table 2). These links are explored more systematically in section 3.

For each scene we derive the two dimensional power spectrum as a function of total wavenumber k, where $k^2 = k_x^2 + k_y^2$ and k_x, k_y are the wavenumbers along the axes of the square scene. The image is first detrended by removing the best-fit plane and then windowed using a Welch window. Spectra for the four test scenes are shown in Fig. 4. We find in general that spectra for both open and closed MCC usually exhibit a peak at some lengthscale (this lengthscale we call λ_1). Power law scaling is generally found at large k. The scale at which the spectrum diverges from the power law we label as λ_2. Closed MCC spectra diverge from the power law at a scale close to the peak scale (i.e. $\lambda_1 \approx \lambda_2$, as in Fig. 4(b) and (c)), but for open MCC the divergence from power law behavior occurs at a scale somewhat smaller than the cell-scale (i.e. $\lambda_1 > \lambda_2$, as in Fig. 4(b) and (c)). Visual inspection of many scenes leads to the conclusion that λ_1 and λ_2 can be interpreted as the approximate cell diameter and typical cloud size respectively. For closed cells these are approximately the same because the gaps between clouds are quite small. Open MCC tends to consist of small clouds that form around the perimeter of a larger cellular structure and so λ_2 is often considerably smaller than λ_1.

Automatic methods are used to determine the lengthscales λ_1 and λ_2 from the power spectral data. Tests using fractally generated scenes with spatial variability characteristics representative of low clouds reveal rms errors in the estimated values of λ_1 of 10-20%, with a tendency for systematic underestimation that increases from approximately 3 km for $\lambda_1 = 20$ km to 6 km for $\lambda_1 = 50$ km. In some cases the power law behavior is either not present or limited to scales similar to the Nyquist frequency (0.5 km^{-1}). In these cases λ_2 is undefined. Similarly, some of the scenes do not contain a peak in the power spectrum other than that introduced artificially by data windowing. In such cases λ_1 is undefined. Table 2 shows values of λ_1 and λ_2 for the example scenes. Note that it is possible that scenes without clearly defined mesoscale cellular convection, such as scene (a) in Fig. 2, can have λ_1 defined. In these cases, roll-like structures give rise to the power spectral peak. Power spectra and their relationship with LWP variance are further explored in section 4.

e. Neural network scene type classification

The LWP pdf and the power spectrum are used together to classify scenes into four categories that encompass the range of mesoscale (1-100 km) structures in low clouds: (i) clouds with no clear identifiable cellularity; (ii) closed MCC; (iii) open MCC; (iv) clouds containing cells but with no clear organization. We use a 3-layer back propagation neural network (Castleman 1996; Atkinson and Tatnall 1997; Clark and Boyce 1999; Schroder et al. 2002), with a feature vector combining 32 elements describing the LWP power spectrum and 40 elements characterizing the LWP pdf. Approximately 1000 scenes were classified by eye as belonging to one of the categories (i)-(iv) above, and this ensemble was randomly split into two to provide training and verification datasets. Training is carried out until the misclassification in the verification dataset ceases to decrease. We obtained a 85-90% classification accuracy for the trained network. Visual inspection shows that misclassified scenes tend to have features common to two categories, i.e. are those that are more difficult to classify for the human observer. The neural network weights derived from the training process are then applied to all MODIS data from the NE and SE Pacific to provide a scene-by-scene classification. Figure 5 shows a selection of sixteen MODIS scenes, arranged by scene type, that have been successfully classified using the neural network algorithm.

f. Reanalysis data

Reanalysis data from NCEP/NCAR (Kistler et al. 2001) are used to investigate links between large-scale meteorology and mesoscale spatial variability. Our methodology is to obtain a set of pertinent reanalysis variables for each of the MODIS scenes analyzed. Reanalysis data are available four times daily on a 2.5×2.5° grid, and include sea surface temperature data (Reynolds and Smith 1994). Trilinear interpolation is used to determine the values of the reanalysis variables at the MODIS scene-center locations and times. We consider three large-scale variables derived from reanalysis in this study: lower tropospheric stability ($LTS = \theta_{700} - \theta_0$, where θ_{700} and θ_0 are the potential temperatures at 700 hPa and the surface respectively); large-scale vertical motion at 850 hPa (w_{850}); surface temperature advection $\mathbf{U} \cdot \nabla SST$, where $\mathbf{U}$ is the surface wind and SST is the sea surface temperature. Because it is known that there exists a sizeable diurnal cycle in surface divergence and subsidence rates above the MBL (Dai and Deser 1999), we use the mean w_{850} for the 24 hour period centered on the time of the MODIS overpass. This is unnecessary for the other reanalysis parameters as their diurnal cycles are much weaker.

3. Cloud fraction and LWP variability

The early work of Barker (1996b) presented the first observational evidence that cloud internal variability and cloud fraction might be linked, with homogeneous clouds also being those with the most extensive cloud cover. However, the limited sample of high resolution satellite images in the Barker study was insufficient to fully explore the relationship between cloud homogeneity and cloud fraction. Similar findings were reported by Pincus et al. (1999) using simultaneous observations from ships and satellite, but no explicit classification by cloud fraction was carried out. The general issue here is to what degree can associations between cloud cover and the internal variability of the cloud can be represented using simple ideas. From a conceptual viewpoint, it is relatively straightforward to argue for such a connection using the simple boundary layer cloud model of Considine et al. (1997) (henceforth CCW), which builds upon ideas from statistical cloud schemes (Sommeria and Deardorff 1977; Mellor 1977) originally intended to parameterize small scale variability in the marine boundary layer. In the CCW model the cloud top height is assumed constant and equal to the inversion base height z_i, and the lifting condensation level (LCL) is assumed to be a random variable with a particular pdf form. The parameter $\zeta = z_i - LCL$ is equal to the cloud thickness h for columns where $\zeta > 0$. Where $\zeta \leq 0$, the MBL is cloud free. Figure 6 demonstrates graphically that for a given pdf form this model yields a relationship between cloud thickness homogeneity for the cloudy columns and cloud fraction, with increased heterogeneity (decreased $\overline{h}/\sigma_h$) associated with lower cloud cover.

Assuming an adiabatic cloud layer, so that LWP and h are related, the CCW model can be expanded to yield the pdf of LWP (Considine et al. 1997; Wood and Taylor 2001). It has been found that a Gaussian pdf form is broadly consistent with observations of both total water content Wood and Field (2000); Larson et al. (2001a) and cloud thickness Wood and Taylor (2001) variability in overcast MBL clouds, but much less is known about these links at smaller CF. It can be shown (e.g. Wood et al. 2002; Jeffery and Austin 2003) that for a Gaussian pdf form, the CCW model yields a unique relationship between the cloud fraction CF and the nondimensional homogeneity parameter $\gamma_{LWP} = (\overline{LWP}/\sigma_{LWP})^2$.

The predictions of the Gaussian-CCW model are tested against all the SE Pacific satellite data in Fig. 7. An almost identical relationship is found for the NE Pacific data (not shown). The general trend of increasing homogeneity with increasing cloud fraction is borne out in the data and the median CF-conditional values of γ_{LWP} are very close to the median value for the Gaussian-CCW model. There does appear to be a slight tendency for the observed values of γ_{LWP} to be greater than those from the model which tests suggest could reflect statistical inhomogeneity within MODIS scenes. An additional demonstration of links between LWP pdf parameters, we examine the relationship between the homogeneity parameter γ_{LWP} and higher moments of the LWP distribution, i.e. the skewness and kurtosis (Fig. 8). The observations show decreasing skewness and kurtosis as γ_{LWP} increases. This is consistent with the example pdfs shown in Fig. 3, with a trend towards more skewed, less bell-shaped structures as the cloud fraction and homogeneity decrease together. Again, the Gaussian-CCW model represents this general trend in the behavior of the higher moments quite faithfully, indicating its utility as a simple description of the links between cloud cover and LWP variability in marine low cloud. In the following section we explore the relationships between the cloud variability and characteristics of the mesoscale cellular convection.

4. Cloud variability and mesoscale cellular convection

In the previous section evidence was presented demonstrating links between the cloud fractional coverage and the cloud LWP pdf. Insight into the role that different convective organization plays in determining the pdf characteristics over the subtropical eastern oceans is provided in Fig. 9 which shows the distribution of cloud mean LWP, cloud fraction CF, and γ_{LWP} for the four categories of scene type discussed in Section 2(e). Much higher cloud fraction and more spatial homogeneity (higher γ_{LWP}) is found for closed MCC compared with open MCC. The no-MCC scenes have a broad distribution of CF and tend to have low mean LWP. These scenes are often found where stratus/stratocumulus sheets are in their early stages of formation.

It is noteworthy that for scenes with $CF > 0.3$, roughly 60% of all scenes are classified as either open or closed MCC, and for $CF > 0.6$, this rises to 75%. This highlights that mesoscale cellular convection is the predominant form for the organization of MBL clouds over the subtropical oceans.

We next examine the scale dependent properties of the cloud fields using spectral analysis. The horizontal scale of the MCC, as defined by λ_1 (Section 2(d) above) is used as a basis for compositing LWP power spectra (Fig. 10). An approximate power law scaling of the high wavenumber tail $k > \lambda_1^{-1}$ with an exponent in the range 1.4-2.0 is found in accordance with previous observations (e.g. Cahalan and Snider 1989; Wood and Taylor 2001). It is also clear that increasing MCC cell size is associated with an increase in variance and that most of the additional variance as λ_1 increases is coming from scales close to the cell scale. This is strong evidence that mesoscale cells are dominating the sub 256 km spatial variability in marine low clouds. This is further confirmed in Fig. 11 which showing a tendency for decreasing homogeneity with increasing cell scale λ_1 for both open and closed MCC. However, although the cell scale appears to be an important factor affecting the cloud structure, it is clear from the fairly broad range of γ_{LWP} at any particular value of λ_1 that variability of the LWP pdf characteristics is not entirely explained by the size of the cells, as open and closed scenes have distinct relationships between $\overline{LWP}$, CF, γ_{LWP} and λ_1. For a particular cell scale, open MCC clouds are considerably more heterogeneous, have lower cloud fraction, and slightly lower cloud mean LWP.

5. Associations between environmental state, MCC and cloud variability

We have seen that the presence or absence of MCC, and the scale of the cells that form when it is present are associated with systematic differences in cloud spatial variability and cover in the subtropical MBL. It is therefore important to examine the environmental states that are associated with the MCC as part of an effort to better understand and parameterize cloud physical properties.

Previous work has shown that low cloud cover in the subtropical MBL is well correlated with lower tropospheric stability (Slingo 1980; Klein and Hartmann 1993; Klein 1997), and in some regions temperature advection (Klein 1997). In addition, the tropospheric subsidence rate (Wyant et al. 2005) has been shown to be a useful classifier of low cloud cover. MBL depth is also expected to be a key property that can potentially impact the energetics and structural properties of low clouds. Little has been reported, however, about the associations between these variables and mesoscale cellular convection and cloud spatial variability.

In this section we examine whether the magnitude and type of mesoscale spatial variability in low clouds is associated with corresponding changes in large scale meteorological factors pertinent to the MBL.

a. Geographical variability

Figure 12 shows median values of the scene mean LWP, the cloud fraction CF, and the homogeneity parameter γ_{LWP} for 2.5°× 2.5° boxes from the entire dataset. Figure 13 shows the median cell size λ_1. The relative frequency of occurrence of the different scene types is shown in Fig. 14, and the mean MBL depth and reanalysis surface winds in Fig. 15.

The increase in γ_{LWP} with increasing cloud fraction explored in Section 3 is clearly seen at the regional level (Fig. 12). There is also the tendency for clouds without MCC near the coasts to have lower mean LWP, although, there is no clear relationship further from shore. In general, both the NE and SE Pacific regions show similar transitions in the spatial variability characteristics of clouds along climatological trajectories. From the near coastal regions off California and Northern Chile which feature shallow MBLs with extensive, homogeneous clouds (Fig. 12), MBLs tend to deepen downstream (Fig. 15), and we observe an increase in the prevalence of closed MCC (Fig. 14) with an increasing cell size (Fig. 13), and increased heterogeneity. Further downstream, open MCC tends to become more prevalent in both regions, although it is more common in the SE Pacific during this season. Over the warmer waters typical of the eastern ocean trades, cellular but disorganized clouds, with low cloud cover and heterogeneous LWP, are most prevalent. Many of these scenes contain trade wind cumulus clouds, but extensive patches of stratiform cloud within these scenes constitute most of the cloud cover. We further explore the links with MBL depth and large scale meterology in the following subsections.

b. MBL depth

The frequency of occurrence of different scene types classified by MBL depth (Fig. 16) confirms the prevalence of clouds without MCC being prevalent in the shallowest MBLs, where MCC is uncommon. The relative frequency of closed MCC peaks at $z_i \approx$ 900 m and then decreases for deeper MBLs. Open MCC is most commonly observed in MBLs in the $1000 < z_i < 1500$ m range, with cellular but disorganized scenes dominating over clearly defined MCC for $z_i > 1500$ m.

In the previous section we saw how the cloud heterogeneity increased with the cell lengthscale. Figure 17 shows, for open and closed MCC separately, the relationship between cell size and MBL depth. For $z_i < 800$ m open MCC rarely occurs, and MCC of either kind is much less common than noncellular clouds. As the MBL deepens, MCC becomes the dominant form and the median cell scale λ_1 increases to aound 30-40 km for $z_i = 1000$ m. Interestingly, the MCC aspect ratio (λ_1:z_i) is typically in the range 30:1 to 40:1 and is quite insensitive to whether the MCC type is open or closed. This result carries consequences for theories describing MCC formation mechanisms, especially those that implicate cloud top radiative cooling as a necessary forcing (e.g. Shao and Randall 1996). At cell sizes of around 50 km, the error analysis (Section 2d) indicates that the estimates of λ_1 are biased low by roughly 6 km. If this is taken into account, the results would indicate a more constant aspect ratio in the range 35:1 to 40:1.

Although there is a tendency for open MCC to become more prevalent than closed MCC as the MBL deepens, for a more controlled study we perform an additional analysis whereby we consider $2.5^\circ \times 2.5^\circ$ boxes where closed and open MCC in total account for over 50% of all scenes (henceforth termed MCC-prevalent boxes). For each of these boxes, we estimate the mean MBL depth (or other large-scale meteorological variables) for open and closed MCC separately and then aggregate these means to estimate a grand mean difference in MBL depth. This analysis reveals that in MCC-prevalent regions, the MBL is actually slightly *shallower* when open MCC is present than when closed MCC is present. However, the difference is comparable to the sampling error, which suggests that the MBL depth is not a key factor controlling the dominant type of MCC that forms in any particular region.

c. Large scale meteorology

Lower tropospheric stability (LTS) was found by Klein and Hartmann (1993) to be strongly correlated with cloud cover in the subtropics at the basinwide spatial scale and on seasonal timescales. We find a similarly high correlation between mean cloud fraction and mean LTS for the $2.5^\circ \times 2.5^\circ$ boxes (r=0.86 and 0.90 for the NE and SE Pacific regions respectively). We find that the mean cloud cover increases by approximately 0.07 for each degree of LTS, which is approximately 20% larger than the value found by Klein and Hartmann (1993).

Given that closed MCC tends to have a considerably higher cloud fraction than open MCC, as discussed in Section 4, one might assume that at MCC-prevalent locations, greater LTS would tend to be associated with closed, as opposed to open MCC. We do find slightly lower LTS, by on average 0.4 K, for open MCC compared with closed MCC in any particular region, but the LTS differences are generally insufficient to explain the much lower cloud fraction, by on average 0.3, for open MCC. We also find negligible systematic differences in temperature advection and 850 hPa vertical velocity for open and closed cells for MCC-prevalent regions. We tested the sensitivity to the choice of reanalysis dataset by comparing results with those from the European Center for Medium Range Weather Forecasting 40-year reanalysis (ERA-40) and found only small quantitative differences. The apparent lack of dependence of the MCC type upon the large scale meteorology (and MBL depth) could be caused by unreliable reanalysis data, but this is unlikely because we find good correlations (up to r=0.6) between lower tropospheric stability and MODIS cloud fraction on synoptic timescales (2-30 days) in accordance with Klein (1997) (not shown) which suggests that the reanalysis data is reasonably accurate at capturing the synoptic scale variability over the subtropical eastern oceans. Physical reasons for the insensitivity of MCC type to large scale meteorology and MBL depth are discussed below.

6. Discussion and conclusions

In this study we have examined characteristics of the spatial variability of cloud liquid water path LWP in low clouds over the eastern subtropical oceans. Our analysis focuses upon the statistics of approximately 20000 256×256 km MODIS scenes containing exclusively low cloud. We identified connections between the cloud fraction and the pdf of LWP, including the tendency for heterogeneity to increase as cloud fraction decreases, and find that the observed behavior is broadly consistent with a Gaussian model of cloud thickness. If this idea were applied to each grid cell of a global model, the pdf cloud be used to predict the average radiation and precipitation fluxes (Cahalan et al. 1994; Larson et al. 2001b) within the cell.

We have classified the scenes according to their structural properties and the pdf of liquid water path. Four categories emerged: unstructured clouds; closed mesoscale cellular convection (MCC); open celled MCC; and cellular but disorganized convection. The results indicate that mesoscale cellular convection (MCC) is extremely common over the eastern subtropical oceans, and that scenes without MCC are quite rare and generally limited to near coastal regions where the MBL is shallow. The findings provide a quantitative corroboration of the climatology of open and closed cellular convection suggested by Agee et al. (1973). Importantly, cloud fraction and spatial variability are linked to the presence or absence of mesoscale cellular convection, and its spatial scale. However, further studies are required to determine if MCC is the key driver.

In looking for factors that influence scene variability, we find that the horizontal cell size of the MCC scales well with MBL depth, with aspect ratios typically in the 30:1 to 40:1 range. This scaling, together with the finding that cloud homogeneity and cloud fraction also depend upon the MCC scale, suggests an important role for MBL depth in the physical processes that control the cloud radiative properties. This is corroborated in Fig. 18 which shows that the $2.5{\times}2.5^{\circ}$ mean cloud fraction is as well correlated with the mean MBL depth as it is with the mean lower tropospheric stability.

Our results indicate that neither lower tropospheric stability, temperature advection, or 850 hPa vertical velocity play a major role in determining the type of MCC, which suggests that instability processes within the boundary layer may be the determining factor. The locations where closed and open MCC are most prevalent (Fig. 14), as well as qualitative examination of geostationary satellite imagery, suggest that a MCC usually transitions from closed to open This change often takes the form of small pockets of open cells forming over a few hours within regions of extensive closed cells, which then grow to become extensive areas of open MCC. Observations (Stevens et al. 2005; Comstock et al. 2005; Sharon et al. 2005; Petters et al. 2005) suggest that the transition may be driven by feedbacks involving microphysics and precipitation.

The results presented here demonstrate potential new ways in which satellite and reanalysis data can be combined to examine the spatial variability of low clouds and the large scale meteorological factors that influence it. Further work could include the extension of this dataset to longer timescales to elucidate the physical mechanisms responsible for the organization of mesoscale cellular convection, cloud fraction, and variability in the marine boundary layer on seasonal timescales.

7. Acknowledgements

The author would like to thank the reviewers for their constructive and insightful comments which helped improve the quality of this paper. The work has benefited through fruitful discussions with Philip Austin and Christopher Bretherton. Funding for this work was provided by the NASA EOS Grant NAGS5-10624 (*Climate Processes over the Oceans*).

References

Ackerman, S. A., K. Strabala, P. Menzel, R. Frey, C. Moeller, L. Gumley, B. Baum, S. Wetzel Seeman, and H. Zhang: 2002, Discriminating clear-sky from cloud with modis. MODIS Algorithm Theoretical Basis Document MOD35 ATBD-MOD-06, NASA.

Agee, E. M., T. S. Chen, and K. E. Dowell: 1973, A review of mesoscale cellular convection. *Bull. Amer. Meteorol. Soc.*, **54**, 1004–1012.

Atkinson, B. W. and J. W. Zhang: 1996, Mesoscale shallow convection in the atmosphere. *Rev. Geophys.*, **34**, 403–431.

Atkinson, P. M. and A. R. L. Tatnall: 1997, Neural networks in remote sensing. *Int. J. Remote Sensing*, **18**, 699–709.

Barker, H. W.: 1996a, A parameterization for computing grid-averaged solar fluxes for inhomogeneous marine boundary layer clouds. Part 1: Methodology and homogeneous biases. *J. Atmos. Sci.*, **53**, 2289–2303.

— 1996b, A parameterization for computing grid-averaged solar fluxes for inhomogeneous marine boundary layer clouds. Part 2: Validation using satellite data. *J. Atmos. Sci.*, **53**, 2304–2316.

Brenguier, J. L., P. Y. Chuang, Y. Fouquart, D. W. Johnson, F. Parol, H. Pawlowska, J. Pelon, L. Schuller, F. Schroder, and J. Snider: 2000, An overview of the ACE-2 cloudycolumn closure experiment. *Tellus*, **52B**, 815–827.

Cahalan, R. F., W. Ridgway, W. J. Wiscombe, T. L. Bell, and J. B. Snider: 1994, The albedo of fractal stratocumulus clouds. *J. Atmos. Sci.*, **51**, 2434–2455.

Cahalan, R. F. and J. B. Snider: 1989, Marine stratocumulus structure. *Rem. Sens. Environ.*, **28**, 95–107.

Castleman, K. R.: 1996, *Digital image processing*. Prentice Hall.

Clark, C. and J. Boyce: 1999, The detection of ship trail clouds by artificial neural network. *Int. J. Remote Sensing*, **20**, 711–726.

Comstock, K., S. E. Yuter, R. Wood, and C. S. Bretherton: 2005, Dissection of drizzling stratocumulus using radar observations. *J. Atmos. Sci.*, in preparation.

Considine, G., J. A. Curry, and B. Wielicki: 1997, Modeling cloud fraction and horizontal variability in marine boundary layer clouds. *J. Geophys. Res.*, **102**, 13517–13525.

Dai, A. and C. Deser: 1999, Diurnal and semidiurnal variations in global surface wind and divergence fields. *J. Geophys. Res.*, **104**, 31109–31125.

Davis, A., A. Marshak, W. Wiscombe, and R. Cahahlan: 1996, Scale invariance of liquid water distributions in marine stratocumulus. Part 1: Spectral properties and strationarity issues. *J. Atmos. Sci.*, **53**, 1538–1558.

Han, Q., W. B. Rossow, and A. A. Lacis: 1994, Near global survey of effective droplet radii in liquid water clouds using isccp data. *J. Clim.*, **7**, 465–497.

Jeffery, C. A. and P. H. Austin: 2003, Unified treatment of the thermodynamic and optical variability of unresolved low clouds. *J. Atmos. Sci.*, **60**, 1621–1631.

King, M. D., Y. Kaufman, W. P. Menzel, and D. Tanré: 1992, Remote sensing of cloud, aerosol, and water vapor properties from the moderate resolution imaging spectroradiometer (modis). *IEEE Trans. Geosci. Rem. Sens.*, **30**, 2–27.

King, M. D., W. P. Menzel, and Y. Kaufman: 2003, Cloud and aerosol properties, precipitable water, and profiles of temperature and water vapor from modis. *IEEE Trans. Geosci. Rem. Sens.*, **41**, 442–458.

King, M. D., S.-C. Tsay, S. E. Platnick, M. Wang, and K.-N. Liou: 1997, Cloud retrieval algorithms for modis: Optical thickness, effective particle radius, and thermodynamic phase. MODIS Algorithm Theoretical Basis Document ATBD-MOD-05, NASA.

Kistler, R., E. Kalnay, W. Collins, S. Sana, G. White, J. Woolen, M. Chelliah, W. Ebisuzaki, M. Kanamitsu, V. Kousky, H. van den Dool, R. Jenne, and M. Fiorino: 2001, The ncep/ncar 50-year reanalysis. *Bull. Am. Meteorol. Soc.*, **82**, 247–267.

Klein, S. A.: 1997, Synoptic variability of low-cloud properties and meteorological parameters in the subtropical trade wind boundary layer. *J. Climate*, **10**, 2018–2039.

Klein, S. A. and D. L. Hartmann: 1993, The seasonal cycle of low stratiform clouds. *J. Climate,*, **6**, 1588–1606.

Larson, V. E., R. Wood, P. R. Field, J.-C. Golaz, T. H. Vonder Haar, and W. R. Cotton: 2001a, Small-scale and mesoscale variability of scalars in cloudy boundary layers: one dimensional probability density functions. *J. Atmos. Sci.*, **58**, 1978–1994.

— 2001b, Systematic biases in the microphysics and thermodynamics of numerical models that ignore subgrid-scale variability. *J. Atmos. Sci.*, **58**, 1117–1128.

Ma, X., Z. Wan, C. Moeller, W. Menzel, L. Gumley, and Y. Zhang: 2000, Retrieval of geophysical parameters from moderate resolution imaging spectroradiometer thermal infrared data: evaluation of a two-step physical algorithm. *Appl. Optics*, **39**, 3537–3550.

Marshak, A., A. Davis, W. Wiscombe, and R. Cahalan: 1997, Scale invariance in liquid water distributions in marine stratocumulus. Part II: multifractal properties and intermittency issues. *J. Atmos. Sci.*, **54**, 1423–1444.

Mellor, G. L.: 1977, The Gaussian cloud model relations. *J. Atmos. Sci.*, **34**, 356–358.

Nicholls, S. and J. Leighton: 1986, An observational study of the structure of stratiform cloud sheets: Part i. structure. *Quart. J. Roy. Meteorol. Soc.*, **112**, 431–460.

Oreopoulos, L. and R. Davies: 1998a, Plane parallel albedo biases from satellite observations. Part I: Dependence on resolution and other factors. *J. Clim.*, **11**, 919–932.

— 1998b, Plane parallel albedo biases from satellite observations. Part II: Parameterizations for bias removal. *J. Clim.*, **11**, 933–944.

Park, S., C. B. Leovy, and M. A. Rozendaal: 2004, A new single column marine boundary layer cloud model. *J. Atmos. Sci.*, submitted.

Petters, M. D., J. R. Snider, B. Stevens, G. Vali, I. Faloona, and L. Russell: 2005, Accumulation mode aerosol, pockets of open cells, and particle nucleation in the remote subtropical pacific marine boundary layer. *J. Geophys. Res.*, in review.

Pincus, R. and S. A. Klein: 2000, Unresolved spatial variability and microphysical process rates in large scale models. *J. Geophys. Res.*, **105**, 27059–27066.

Pincus, R., S. A. McFarlane, and S. A. Klein: 1999, Albedo bias and the horizontal variability of clouds in subtropical marine boundary layers: observations from ships and satellites. *J. Geophys. Res.*, **104**, 6183–6191.

Pincus, R., M. Szczodrak, J. Gu, and P. Austin: 1995, Uncertainty in cloud optical depth estimates made from satellite radiance measurements. *J. Clim.*, **8**, 1453–1462.

Reynolds, R. W. and T. M. Smith: 1994, Improved global sea surface temperature analyses using optimum interpolation. *J. Clim.*, **7**, 929–948.

Rossow, W. B., C. Delo, and B. Cairns: 2002, Implications of the observed mesoscale variations of clouds for earth's radiation budget. *J. Clim.*, **15**, 557–585.

Rossow, W. B. and R. A. Schiffer: 1991, ISCCP cloud data products. *Bull. Am. Meteorol. Soc.*, **72**, 2–20.

Rotstayn, L. D.: 2000, On the "tuning" of autoconversion parameterizations in climate models. *J. Geophys. Res.*, **105**, 15,495–15,507.

Schroder, M., R. Bennartz, L. Schuller, R. Preusker, P. Albert, and J. Fischer: 2002, Generating cloudmasks in spatial high-resolution observations of clouds using texture and radiance information. *Int. J. Remote Sensing*, **23**, 4247–4261.

Shao, Q. and D. A. Randall: 1996, Closed mesoscale cellular convection driven by cloud-top radiative cooling. *J. Atmos. Sci.*, **53**, 2144–2165.

Sharon, T. M., B. A. Albrecht, H. Jonsson, P. Minnis, M. M. Khaiyer, T. M. VanReken, J. Seinfeld, and R. Flagan: 2005, Aerosol and cloud microphysical characteristics of rifts and gradients in maritime stratocumulus clouds. *J. Atmos. Sci.*, in press.

Slingo, J. M.: 1980, A cloud parameterization scheme derived from GATE data for use with a numerical model. *Quart. J. Roy. Meteorol. Soc.*, **106**, 774–770.

Smith, R. N. B.: 1990, A scheme for predicting layer clouds and their water content in a general circulation model. *Q. J. R. Meteorol. Soc.*, **116**, 435–460.

Sommeria, G. and J. W. Deardorff: 1977, Subgrid-scale condensation in models of nonprecipitating clouds. *J. Atmos. Sci.*, **34**, 344–355.

Stevens, B., G. Vali, K. Comstock, R. Wood, M. VanZanten, P. H. Austin, and D. H. Bretherton C. S.ãnd, Lenschow: 2005, Pockets of open cells (POCs) and drizzle in marine stratocumulus. *Bull. Am. Meteor. Soc.*, **86**, 51–57.

Tompkins, A. M.: 2002, A prognostic parameterization for the subgrid-scale variability of water vapor and clouds in large-scale models and its use to diagnose cloud cover. *J. Atmos. Sci.*, **59**, 1917–1942.

Wood, R.: 2005, Drizzle in stratiform boundary layer clouds: Part I. Vertical and horizontal structure. *J. Atmos. Sci.*, in press.

Wood, R. and C. S. Bretherton: 2004, Boundary layer depth, entrainment and decoupling in the cloud-capped subtropical and tropical marine boundary layer. *J. Clim.*, **17**, 3576–3588.

Wood, R. and P. R. Field: 2000, Relationships between total water, condensed water, and cloud fraction in stratiform clouds examined using aircraft data. *J. Atmos. Sci.*, **57**, 1888–1905.

Wood, R., P. R. Field, and W. R. Cotton: 2002, Autoconversion rate bias in boundary layer cloud parameterizations. *Atmos. Res.*, **65**, 109–128.

Wood, R. and J. P. Taylor: 2001, Liquid water path variability in unbroken marine stratocumulus. *Quart. J. Roy. Meteorol. Soc.*, **127**, 2635–2662.

Wyant, M. E., C. S. Bretherton, J. T. Bacmeister, J. T. Kiehl, I. M. Held, Z. M. S. A. Klein, and B. A. Soden: 2005, A comparison of tropical cloud properties and responses in gcms using mid-tropospheric vertical velocity. *Clim. Dyn.*, in press.

Figure Captions

Figure 1: The two regions (NE and SE Pacific) in this study. Contours show fraction of 256×256 km scenes containing only warm cloud ($T_{top} > 273$ K). Grayscale shading shows ISCCP mid+high cloud amount for Sept/Oct 1984-1999.

Figure 2: Example scenes of MODIS liquid water path in boundary layer cloud showing wide variability in cloud structure. Each scene size is 256×256 km at 1 km resolution. Image times and locations are given in Table 2.

Figure 3: Examples of LWP pdfs for the four test scenes shown in Fig. 2.

Figure 4: Power spectra calculated using a two dimensional fast Fourier transform for the four example scenes shown in Fig. 2. The unsmoothed spectra are shown using the solid line. Spectra are normalised so that $\int_0^\infty P_{LWP} dk = \sigma^2_{LWP,all}$ where $\sigma_{LWP,all}$ is the standard deviation of LWP (including cloud free regions where $LWP = 0$). Averaged spectra are shown using filled circles and approximate 95% confidence limits are given by the light dotted line. The filled triangle on the wavenumber axis shows the "mean" wavenumber used to determine the power law fit to the large k end of the observed spectra (thick dotted line). The two characteristic lengthscales are defined as λ_1, the wavelength of the highest wavenumber peak in the averaged power spectrum. λ_2, the minimum wavenumber at which the 95% confidence limit of the spectrum exceeds the fitted power law. These scales correspond approximately to cellular diameters and cloud-sizes respectively.

Figure 5: Selection of MODIS scenes categorized by the neural network scene classification type.

Figure 6: Links between nondimensional cloud heterogeneity and cloud fraction for a simple pdf model of cloud thickness variability. The horizontal axis represents the difference in height h between the inversion base height z_i and the lifting condensation level (LCL), so that the shaded areas represent cloudy regions and the unshaded regions are regions without cloud.

Figure 7: Cloud fraction-conditional probability contours (shaded) of γ_{LWP} for all the SE Pacific MODIS scenes. The contours represent 5th, 10th, 25th, 75th, 90th and 95th percentiles. Median CF-conditional values of γ_{LWP} are also shown (filled circles) together with the median values for the Gaussian-CCW model. Note that the unique nature of the $CF - \gamma_{LWP}$ relationship in the Gaussian-CCW model is violated when a minimum LWP threshold is applied, as must be done to properly compare with the MODIS data. This results in some spread in the model $CF - \gamma_{LWP}$ relationship, but that spread is minimal compared with the spread in the MODIS data themselves.

Figure 8: Skewness-γ_{LWP} (a) and kurtosis-γ_{LWP} (b) frequency distribution (contours) from all SE Pacific MODIS scenes. Median γ_{LWP}-conditional values of skewness S_{LWP} and kurtosis K_{LWP} are shown from the data (filled circles) and for the Gaussian-CCW model with a LWP

threshold of 5 g m^{-2}.

Figure 9. Probability distributions, expressed using box-whisker plots (showing percentiles 5, 10, 25, 50, 75, 90 and 95) of (a) $\overline{LWP}$, (b) CF, (c) γ_{LWP}, for the four scene types.

Figure 10: Averaged power spectra four different ranges of the characteristic cell lengthscale λ_1. Vertical gray bars indicate extent of λ_1 ranges used for compositing. Data are taken from the NE Pacific region only; composite spectra are almost identical for the SE Pacific data.

Figure 11: (a) Normalized homgeneity parameter γ_{LWP} probability density function conditional on cell size for all MODIS scenes where λ_1 is defined. Shading is as for Fig. 7; Median value of λ_1-conditional cloud mean liquid water path $\overline{LWP}$ (b); cloud fraction CF (c); homogeneity parameter γ_{LWP} (d), for scenes classified as closed and open mesoscale cellular convection.

Figure 12: Climatological mean value of $\overline{LWP}$ (a,b), CF (c,d), and climatological median value of γ_{LWP} (e,f) for all September/October MODIS scenes in the NE and SE Pacific.

Figure 13: Median values of the characteristic lengthscale for all scenes containing MCC (open or closed) with $CF > 0.2$ for the NE (a) and SE (b) Pacific regions.

Figure 14: Frequency of occurrence of no MCC, closed MCC, open MCC, and cellular but disorganized scene types for the NE and SE Pacific.

Figure 15: Mean MBL depth (contours) and NCEP reanalysis surface winds (arrows) for all warm cloud scenes in the NE (a) and SE (b) Pacific, Sept/Oct 2000.

Figure 16: Frequency of occurrence of the four scene type categories classified by MBL depth z_i.

Figure 17: Median characteristic cell lengthscale λ_1 binned by MBL depth z_i for all MODIS scenes (solid circles) over the NE and SE Pacific. The dotted lines denote aspect ratios of 20:1, 30:1 and 40:1. Error bars indicate the approximate sampling error in the median. The solid line indicates the fit described in the text.

Figure 18: (a) Two-monthly mean values of MODIS scene cloud fraction for each $2.5\times2.5^{\circ}$ region, plotted against (a) mean lower tropospheric stability; (b) mean MBL depth. Data from the SE Pacific region are from south of the equator only where surface sensible heat fluxes do not dominate the MBL energetics. The dotted line in (a) shows the results of Klein and Hartmann (1993) and the dashed line the best fit to the MODIS data for the NE and SE Pacific combined.

Table 1: Details of the regions examined in this study.

Region	Longitude range	Latitude range	Period [mm/dd/yy]	Scenes analyzed [number]
NE Pacific	110-150W	10-50N	08/20/00-10/31/00	7803
SE Pacific	70-120W	30S-10N	09/01/00-10/31/00	12992

Table 2: Characteristics of the four test images shown in Fig. 2. Parameters listed are cloud fraction CF; characteristic scale of the cells λ_1 and of the cloud structures λ_2; mean liquid water path $\overline{LWP}$; the ratio of square of the mean mean to the variance of LWP for for cloudy pixels only (γ_{LWP}); liquid water path skewness S_{LWP}; Scene type (no MCC, N; closed MCC, C; open MCC, O) ; boundary layer depth z_i.

Image	Date	Location [lat,long]	CF	λ_1 [km]	λ_2 [km]	$\overline{LWP}$ [g m^{-2}]	γ	S_{LWP}	Type	z_i [m]
(a)	17 Oct 00	36N,125W	0.99	5.4	N/A[1]	59	5.02	0.51	N	610
(b)	18 Aug 00	30N,131W	0.88	10.9	10.3	64	3.13	1.45	C	760
(c)	18 Aug 00	26N,135W	0.86	38.5	48.2	85	1.35	1.38	C	1100
(d)	13 Oct 00	11S,97W	0.32	35.7	10.1	92	1.24	1.72	O	1020

Notes: [1] Characteristic scale undetermined.

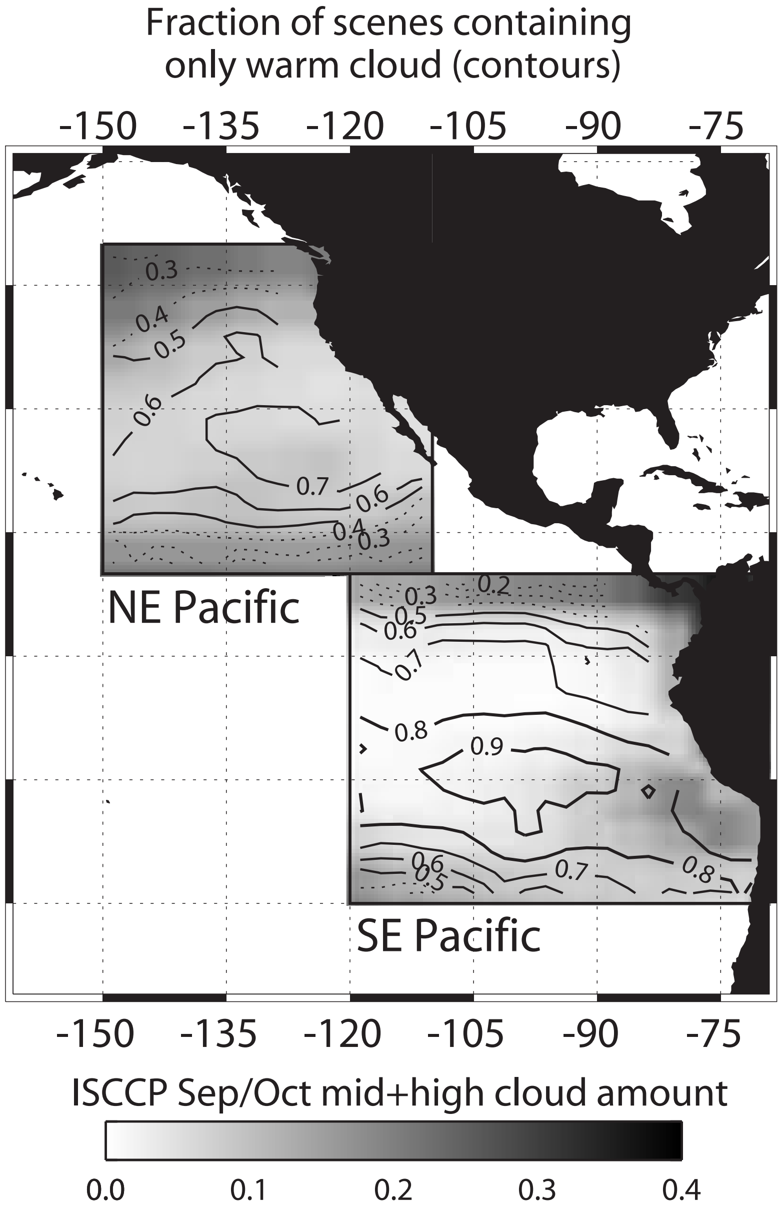
Fraction of scenes containing
only warm cloud (contours)
-150
-135
-120
-105
-90
-75
45
30
15
0
-15
-30
NE Pacific
SE Pacific
ISCCP Sep/Oct mid+high cloud amount
0.0
0.1
0.2
0.3
0.4

Figure 1:

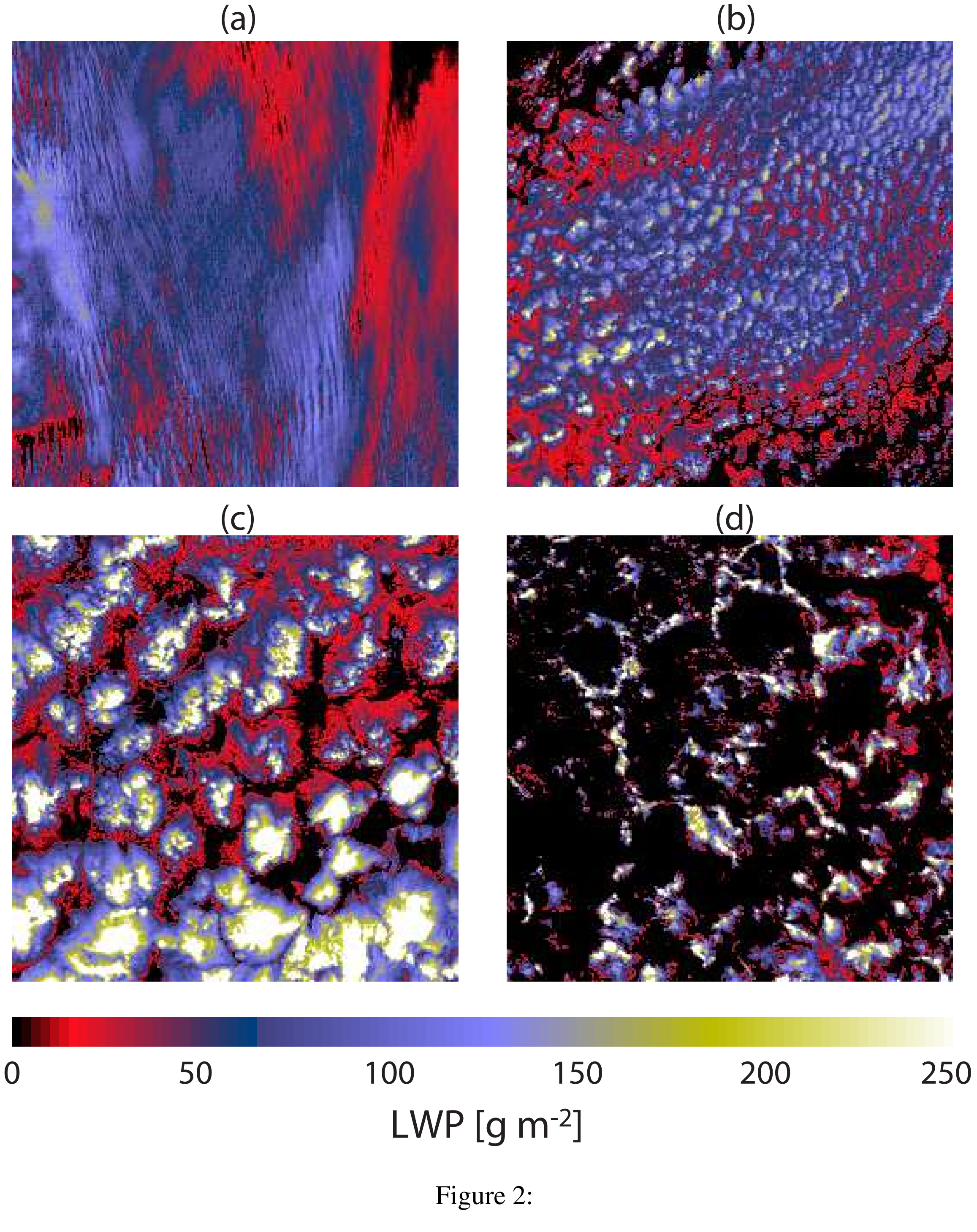

Figure 2:

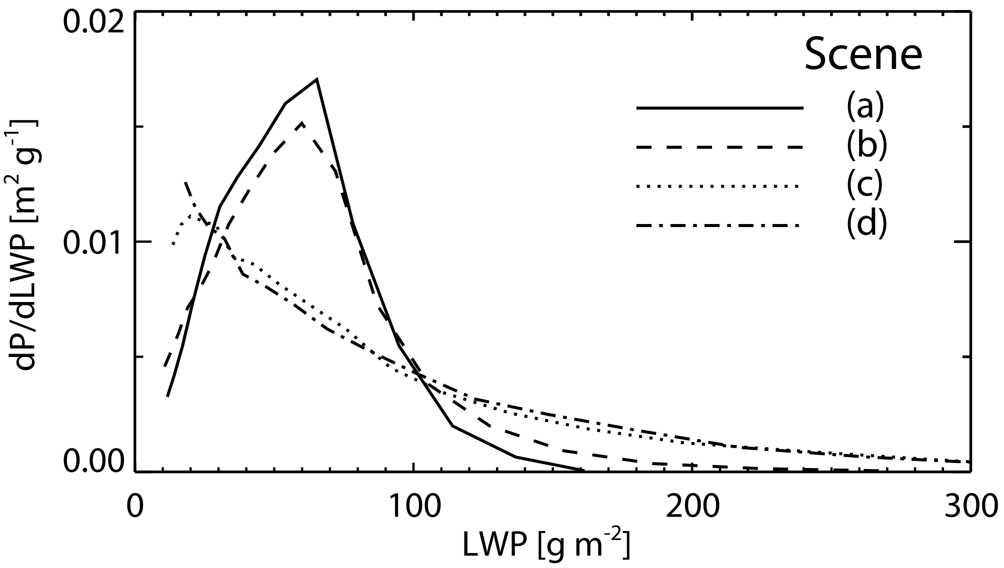

Figure 3:

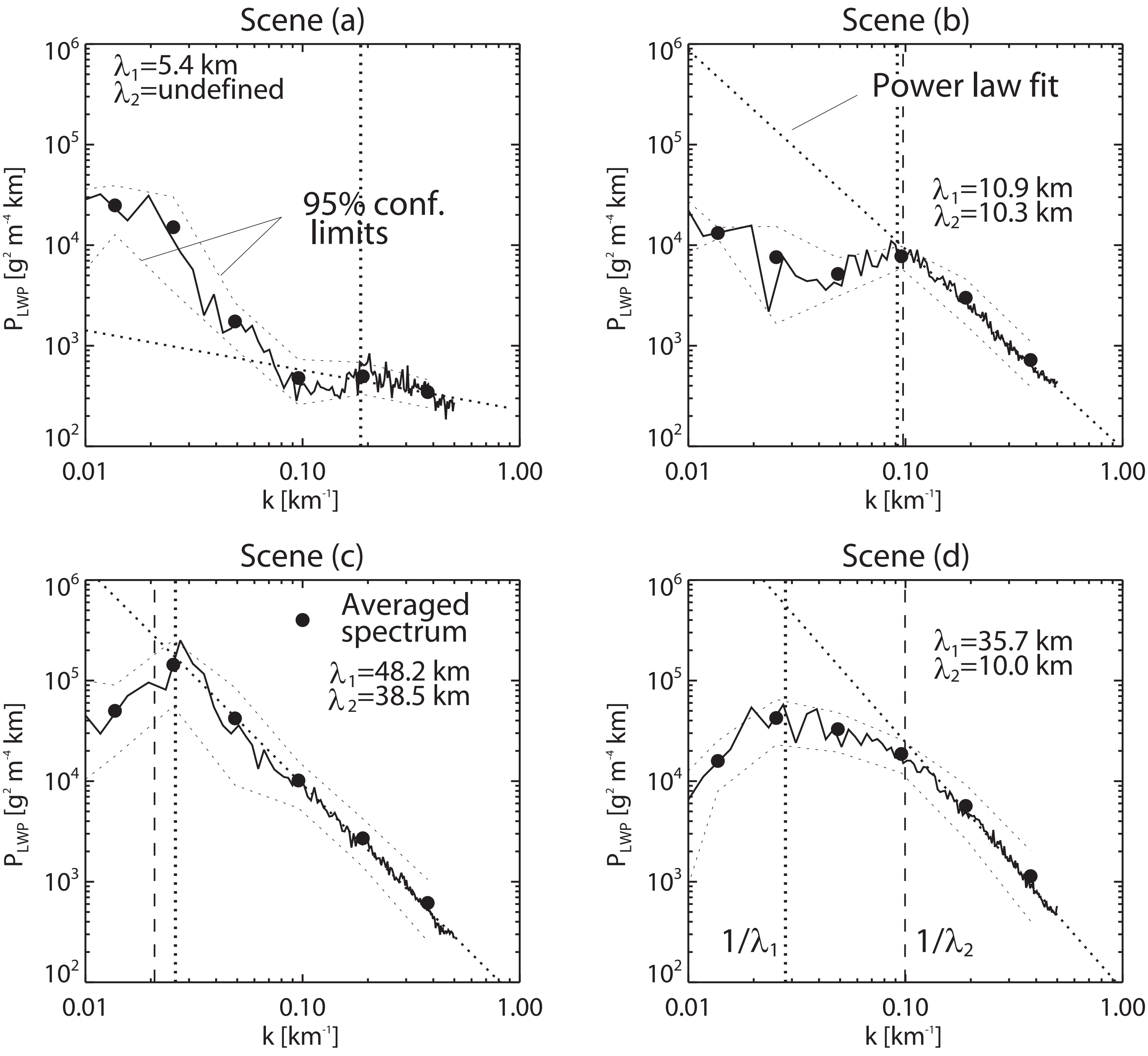

Scene (a)
λ_1=5.4 km
λ_2=undefined
95% conf. limits
Scene (b)
Power law fit
λ_1=10.9 km
λ_2=10.3 km
Scene (c)
Averaged spectrum
λ_1=48.2 km
λ_2=38.5 km
Scene (d)
λ_1=35.7 km
λ_2=10.0 km
$1/\lambda_1$
$1/\lambda_2$
P_{LWP} [g^2 m^{-4} km]
k [km^{-1}]

Figure 4:

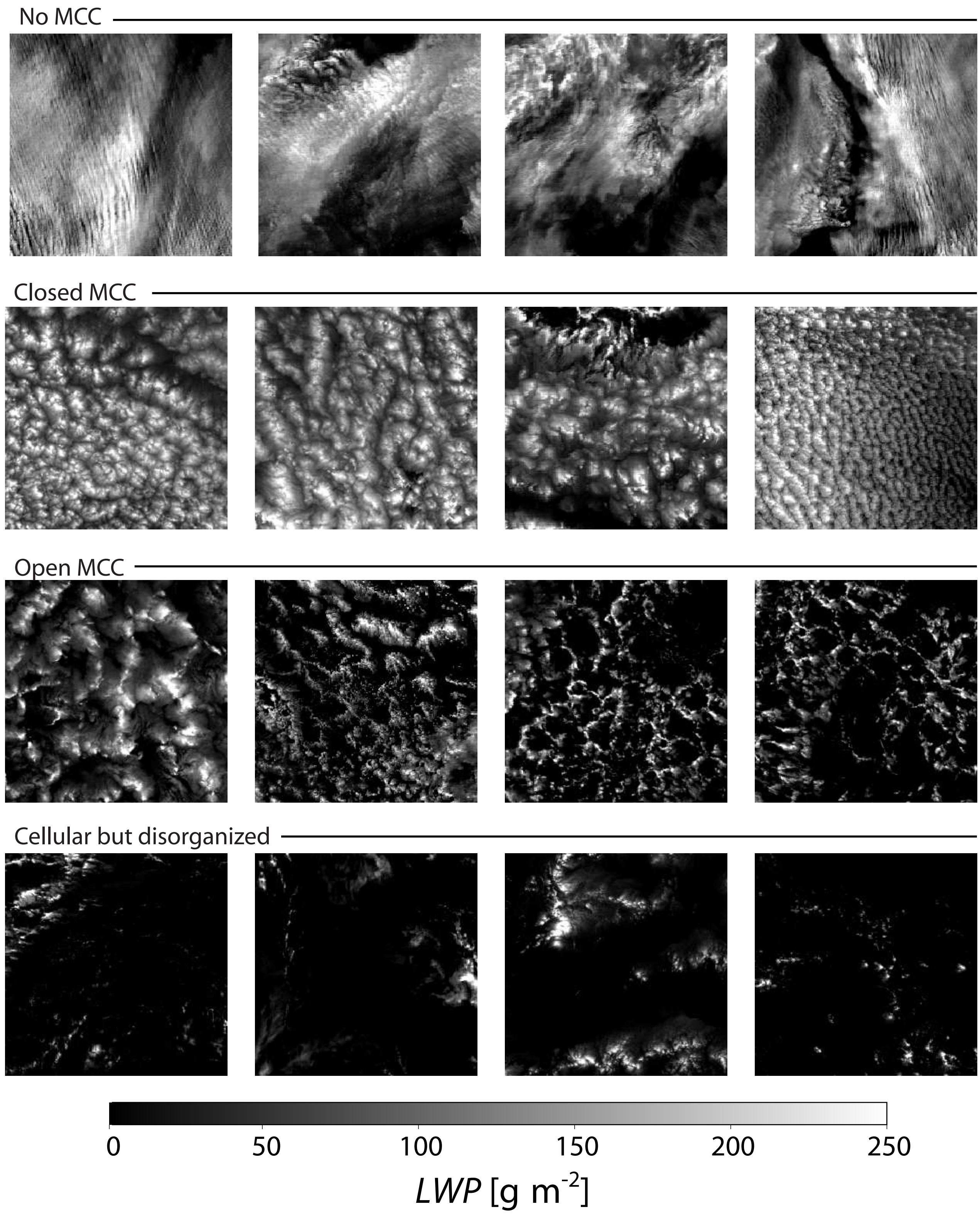
No MCC
Closed MCC
Open MCC
Cellular but disorganized
0
50
100
150
200
250
LWP [g m-2]

Figure 5:

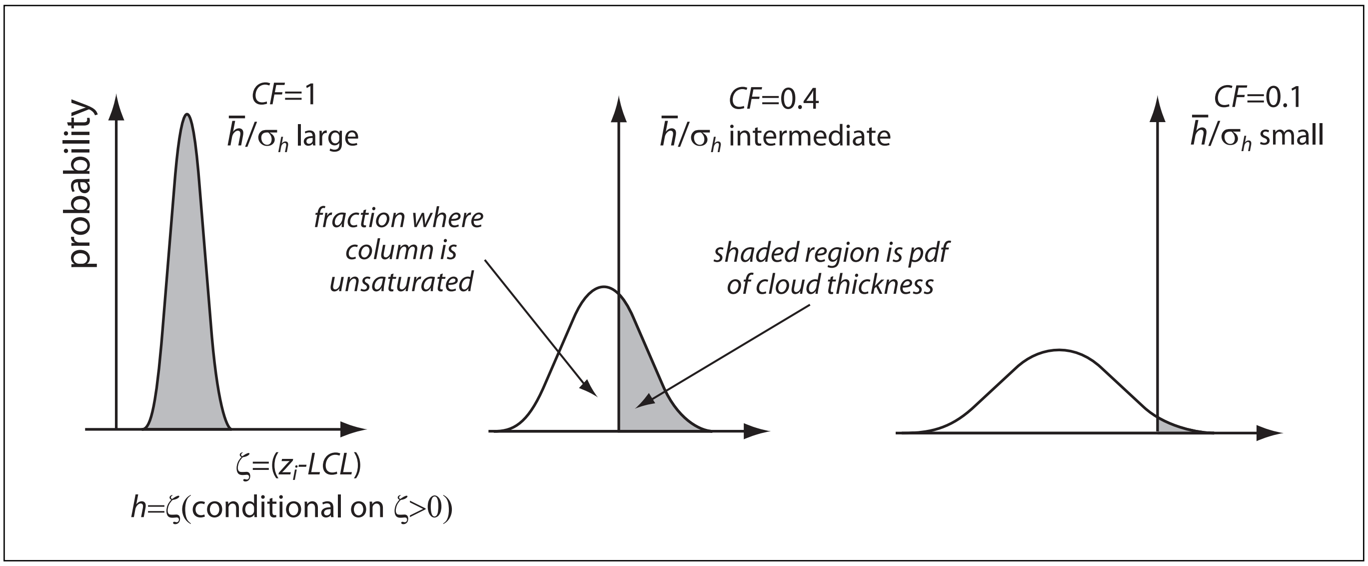

CF=1
$\overline{h}/\sigma_h$ large
probability
ζ=(z_i-LCL)
h=ζ(conditional on ζ>0)
CF=0.4
$\overline{h}/\sigma_h$ intermediate
fraction where column is unsaturated
shaded region is pdf of cloud thickness
CF=0.1
$\overline{h}/\sigma_h$ small

Figure 6:

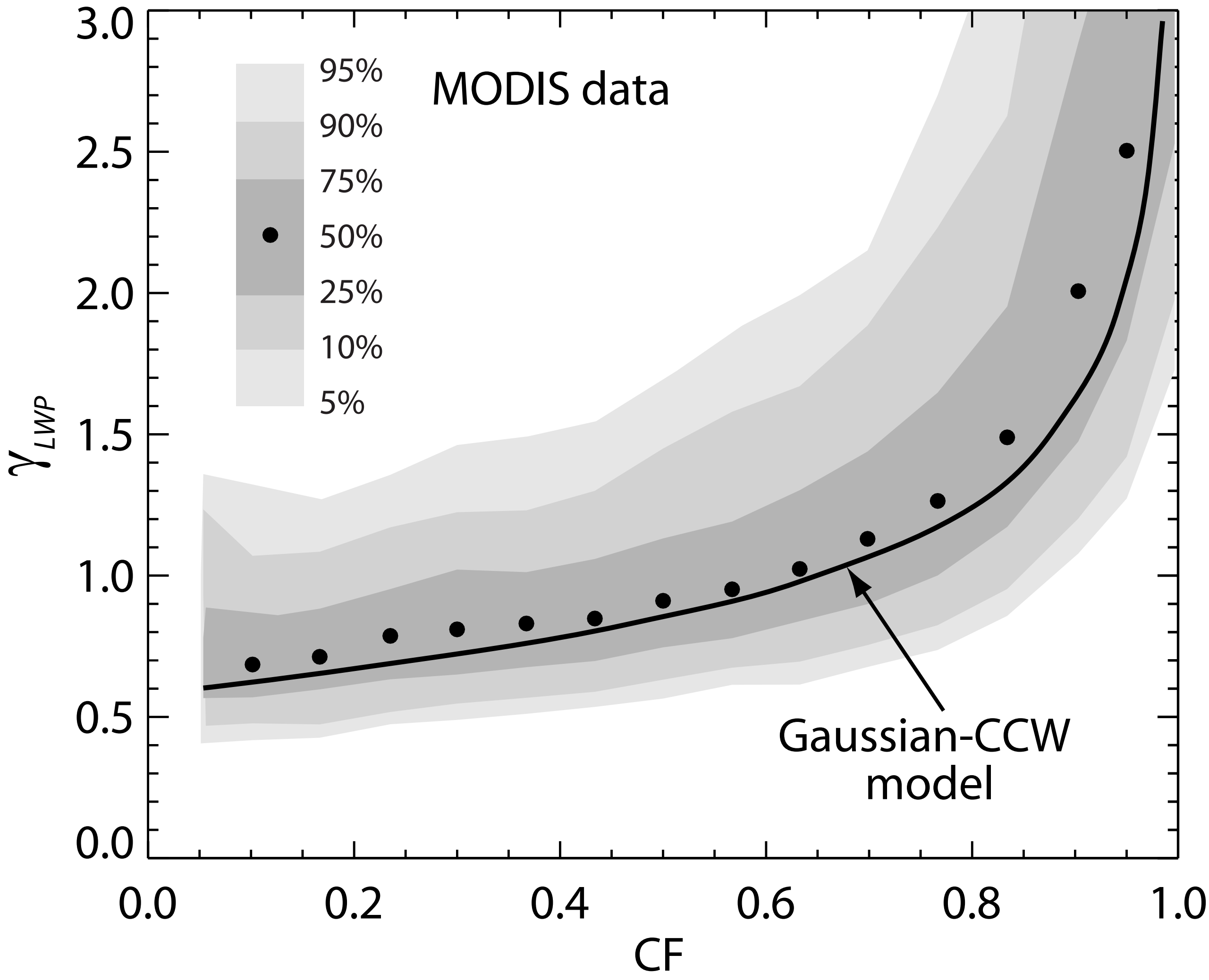

95%
90%
75%
50%
25%
10%
5%
MODIS data
Gaussian-CCW
model
3.0
2.5
2.0
1.5
1.0
0.5
0.0
γ_{LWP}
0.0
0.2
0.4
0.6
0.8
1.0
CF

Figure 7:

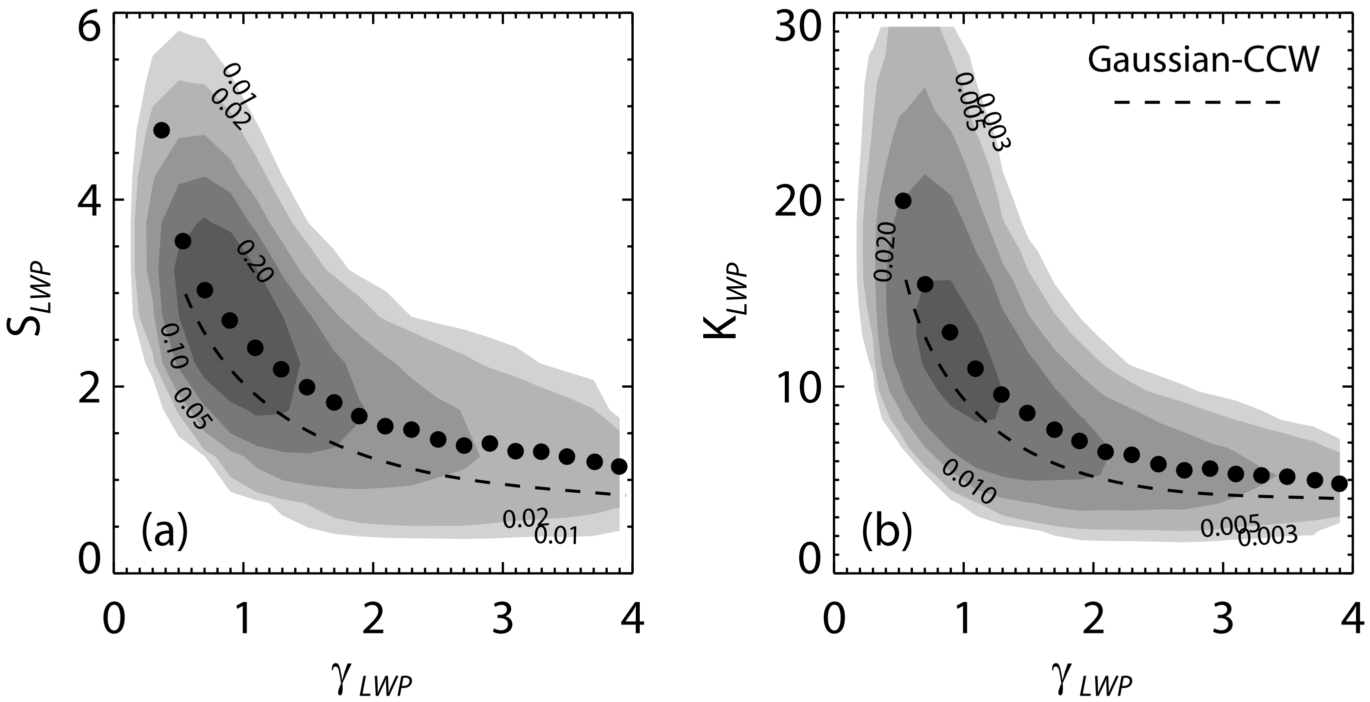

Gaussian-CCW
(a)
(b)
0.01
0.02
0.20
0.10
0.05
0.02
0.01
0.020
0.010
0.005
0.003
S_{LWP}
K_{LWP}
γ_{LWP}
γ_{LWP}

Figure 8:

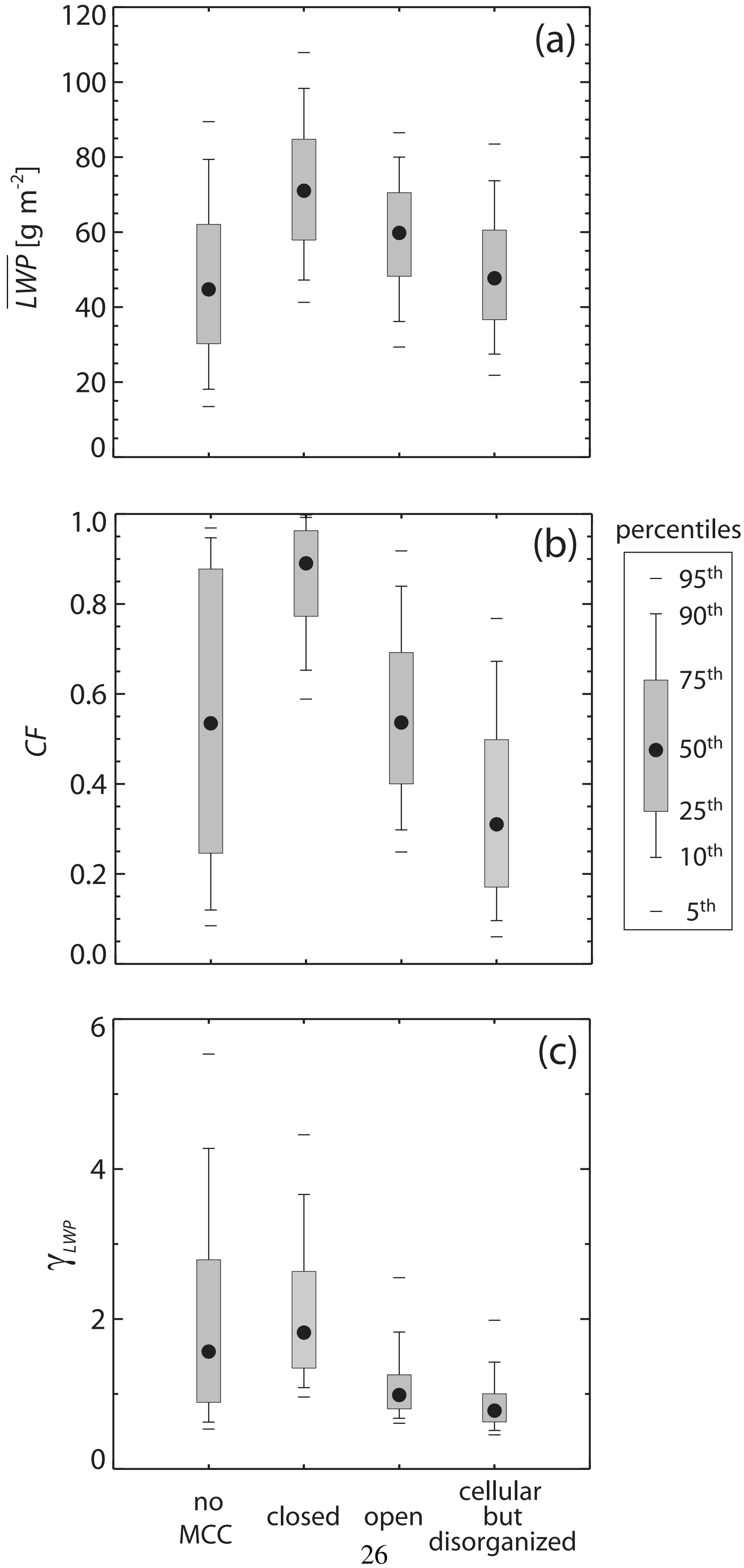

(a)
$\overline{LWP}$ [g m^{-2}]
120
100
80
60
40
20
0
(b)
CF
1.0
0.8
0.6
0.4
0.2
0.0
percentiles
95th
90th
75th
50th
25th
10th
5th
(c)
γ_{LWP}
6
4
2
0
no MCC
closed
open
cellular but disorganized

Figure 9:

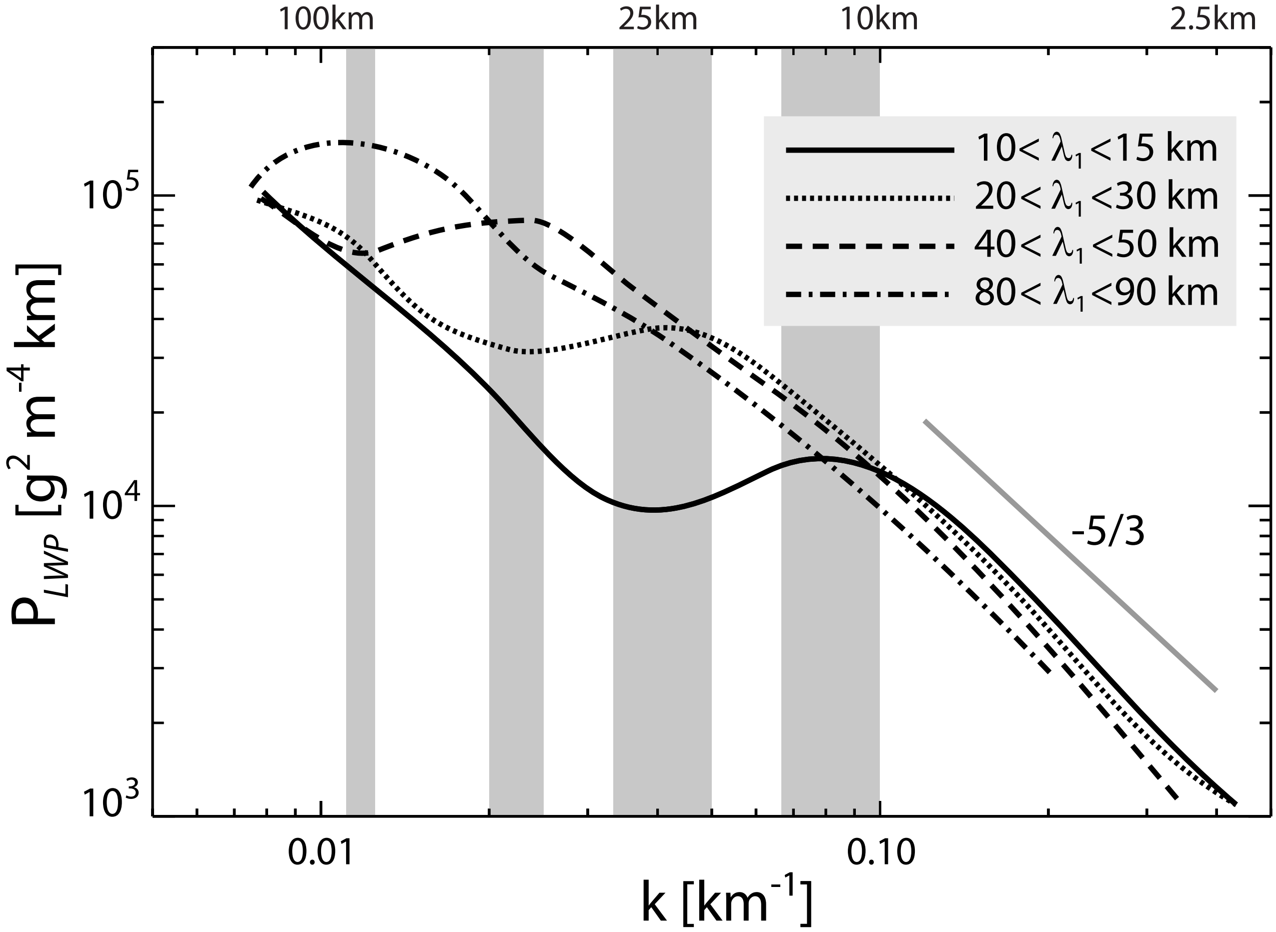

100km
25km
10km
2.5km
10< λ1 <15 km
20< λ1 <30 km
40< λ1 <50 km
80< λ1 <90 km
-5/3
10^5
10^4
10^3
P_{LWP} [g^2 m^{-4} km]
0.01
0.10
k [km^{-1}]

Figure 10:

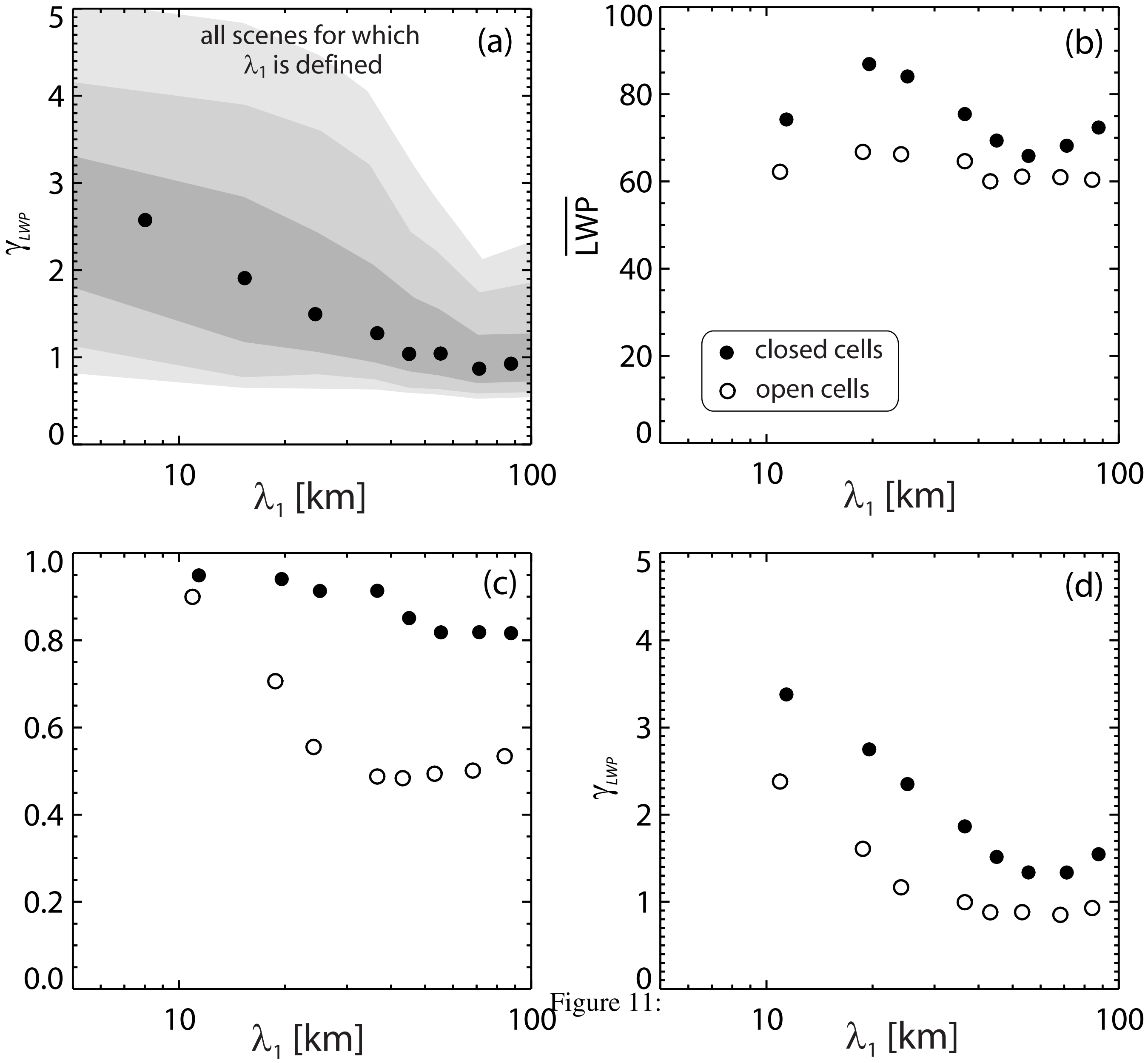
all scenes for which
λ1 is defined
(a)
(b)
(c)
(d)
closed cells
open cells
γ_{LWP}
$\overline{LWP}$
CF
λ_1 [km]

Figure 11:

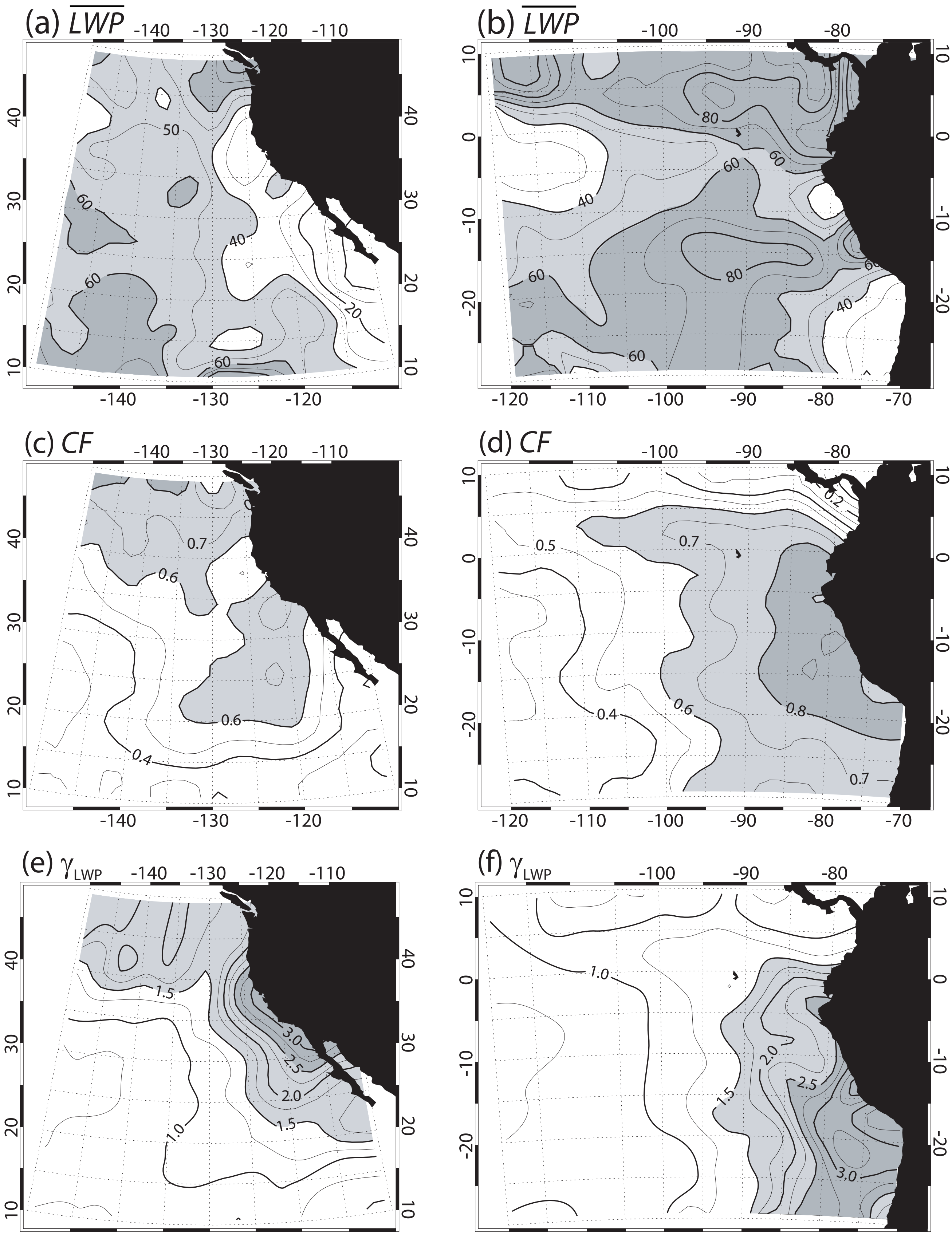

Figure 12:

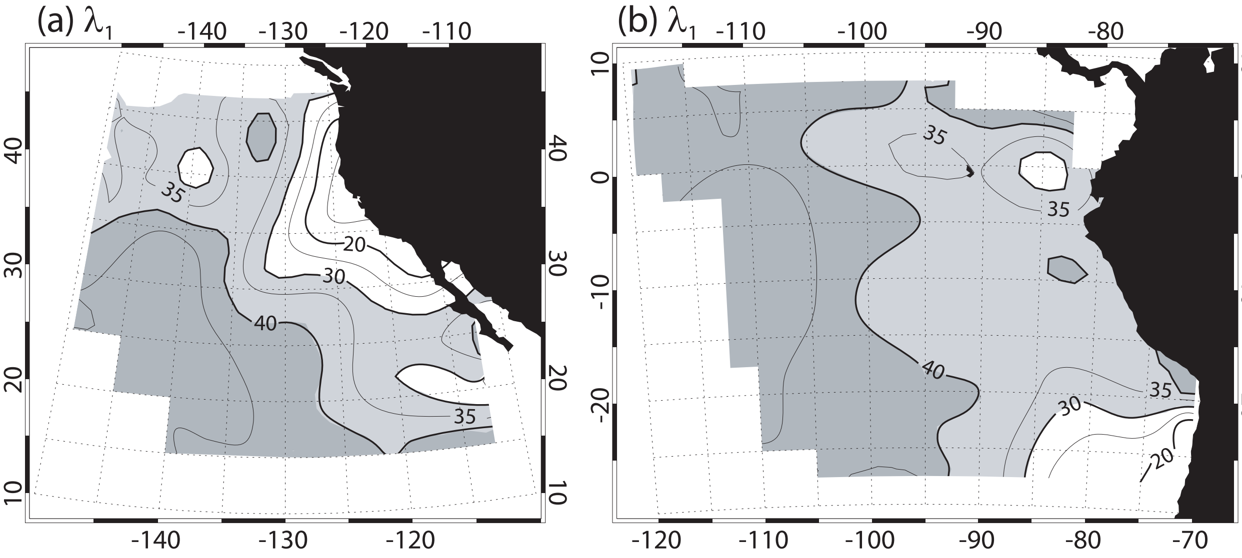

(a) λ_1
-140
-130
-120
-110
40
30
20
10
35
20
30
40
35
(b) λ_1
-110
-100
-90
-80
10
0
-10
-20
35
35
40
35
30
20
-120
-70

Figure 13:

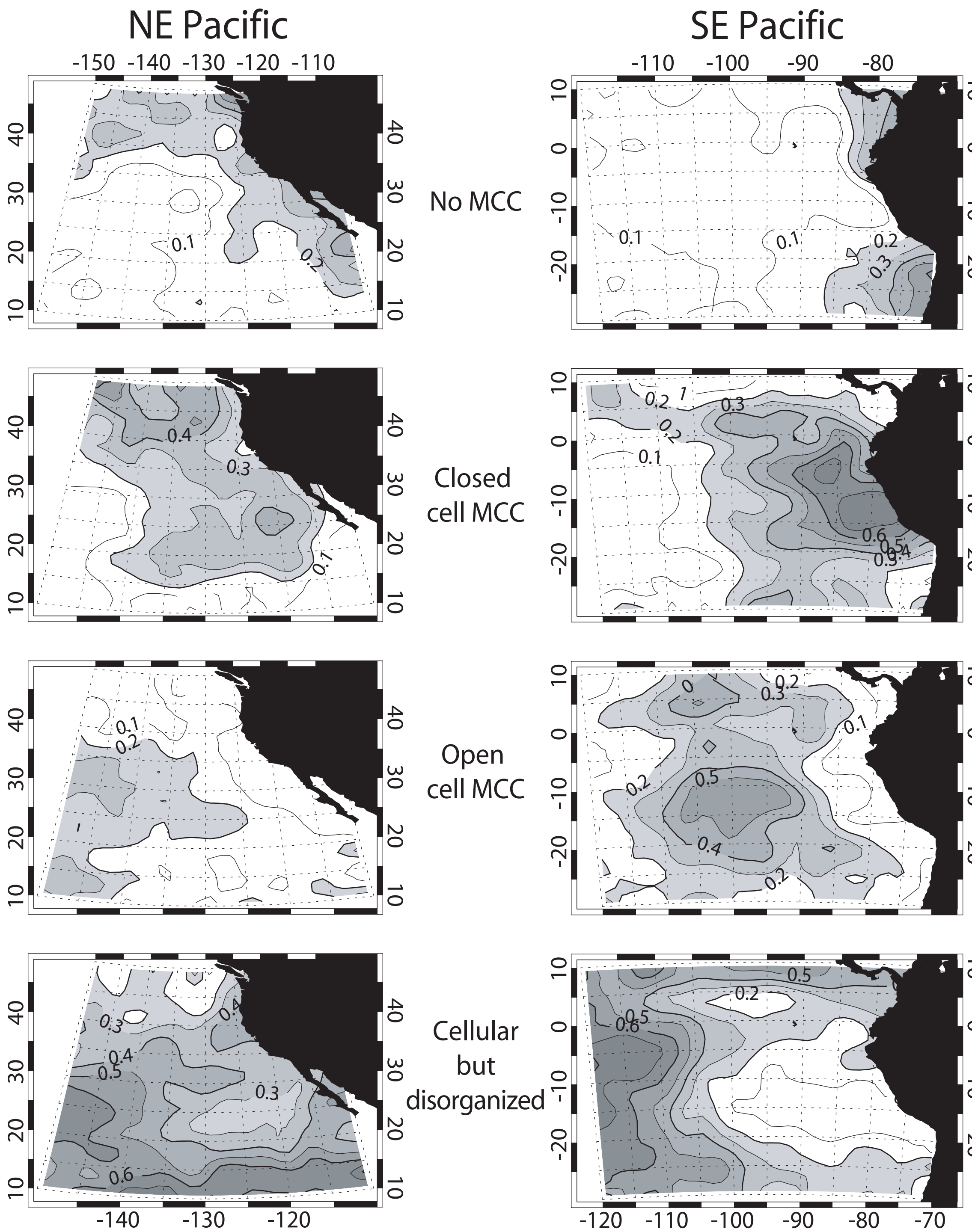
NE Pacific
SE Pacific
No MCC
Closed cell MCC
Open cell MCC
Cellular but disorganized
-150 -140 -130 -120 -110
-110 -100 -90 -80
-140 -130 -120
-120 -110 -100 -90 -80 -70

Figure 14:

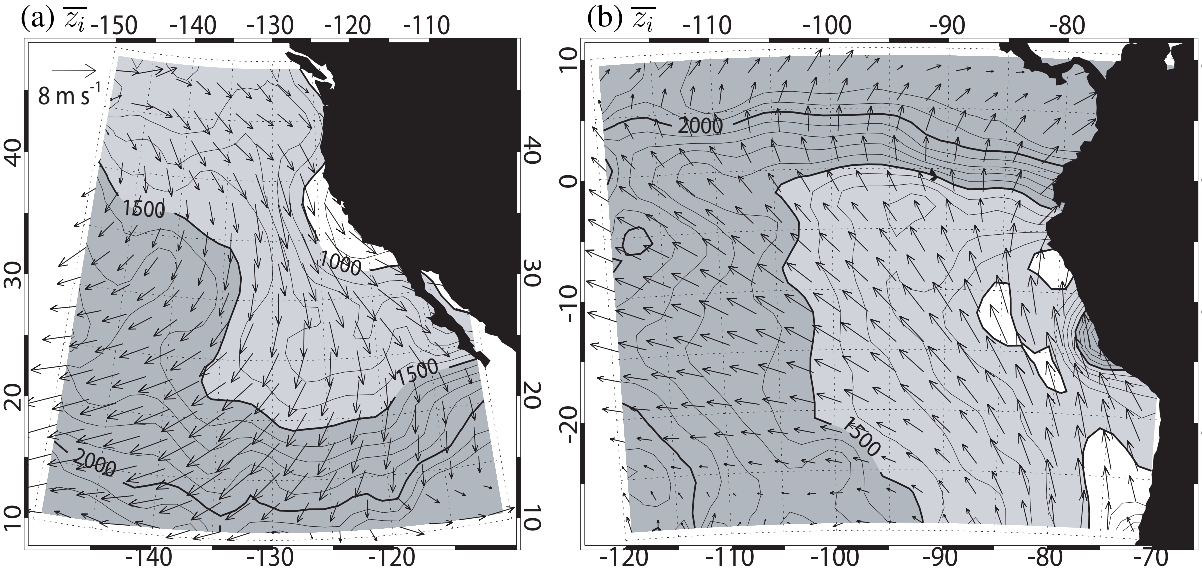
(a) $\overline{z_i}$
8 m s-1
1500
1000
1500
2000
(b) $\overline{z_i}$
2000
1500

Figure 15:

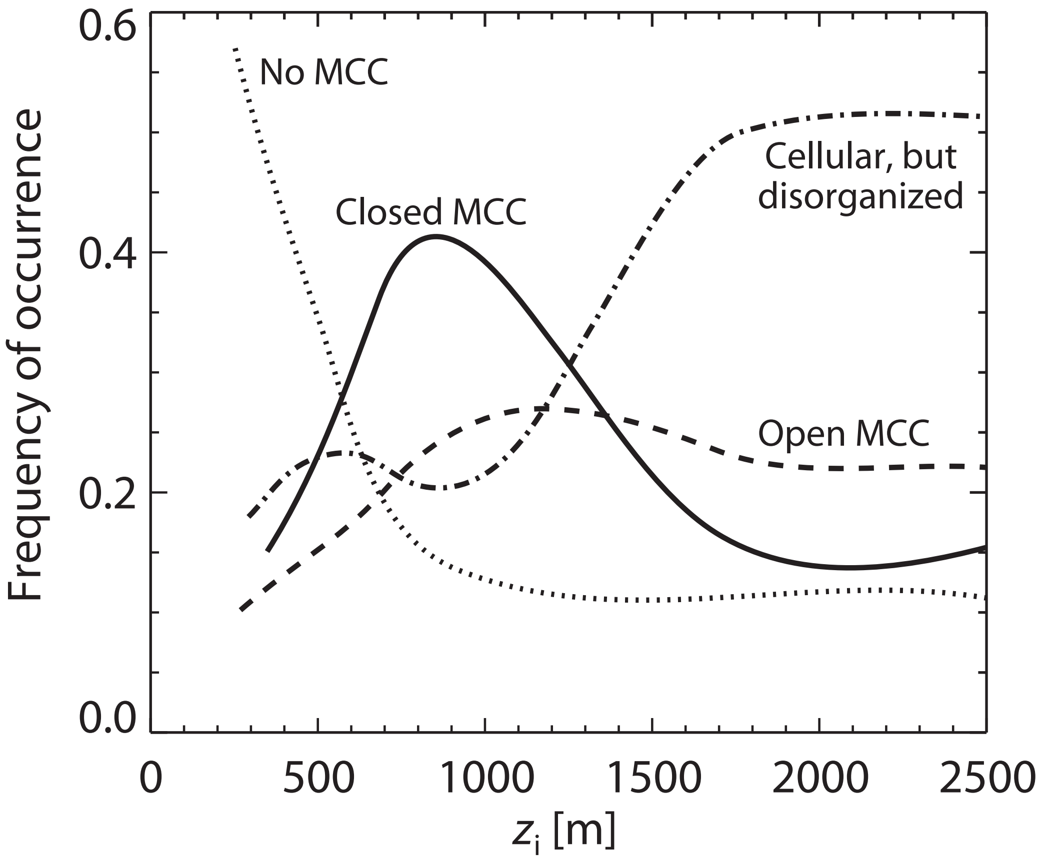

Frequency of occurrence
0.6
0.4
0.2
0.0
No MCC
Closed MCC
Cellular, but disorganized
Open MCC
0
500
1000
1500
2000
2500
z_i [m]

Figure 16:

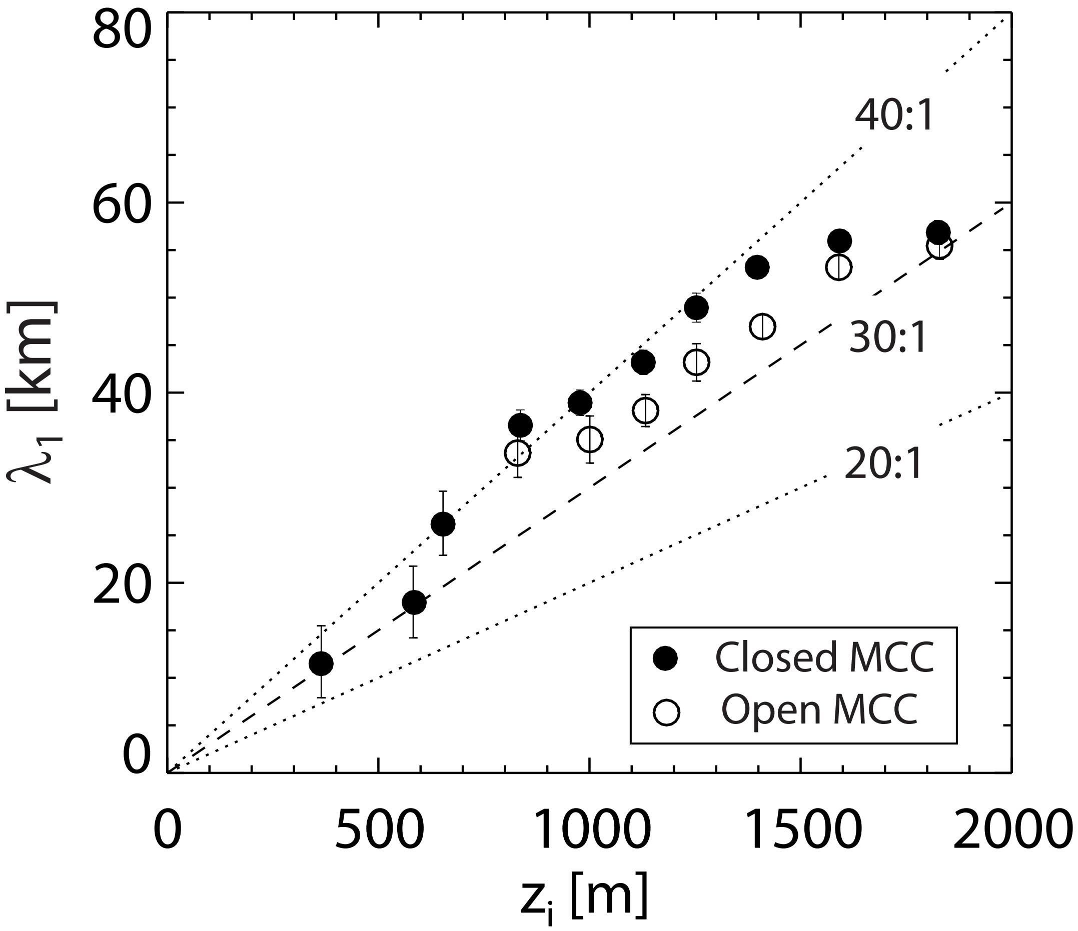
80
60
40
20
0
40:1
30:1
20:1
Closed MCC
Open MCC
0
500
1000
1500
2000
λ_1 [km]
z_i [m]

Figure 17:

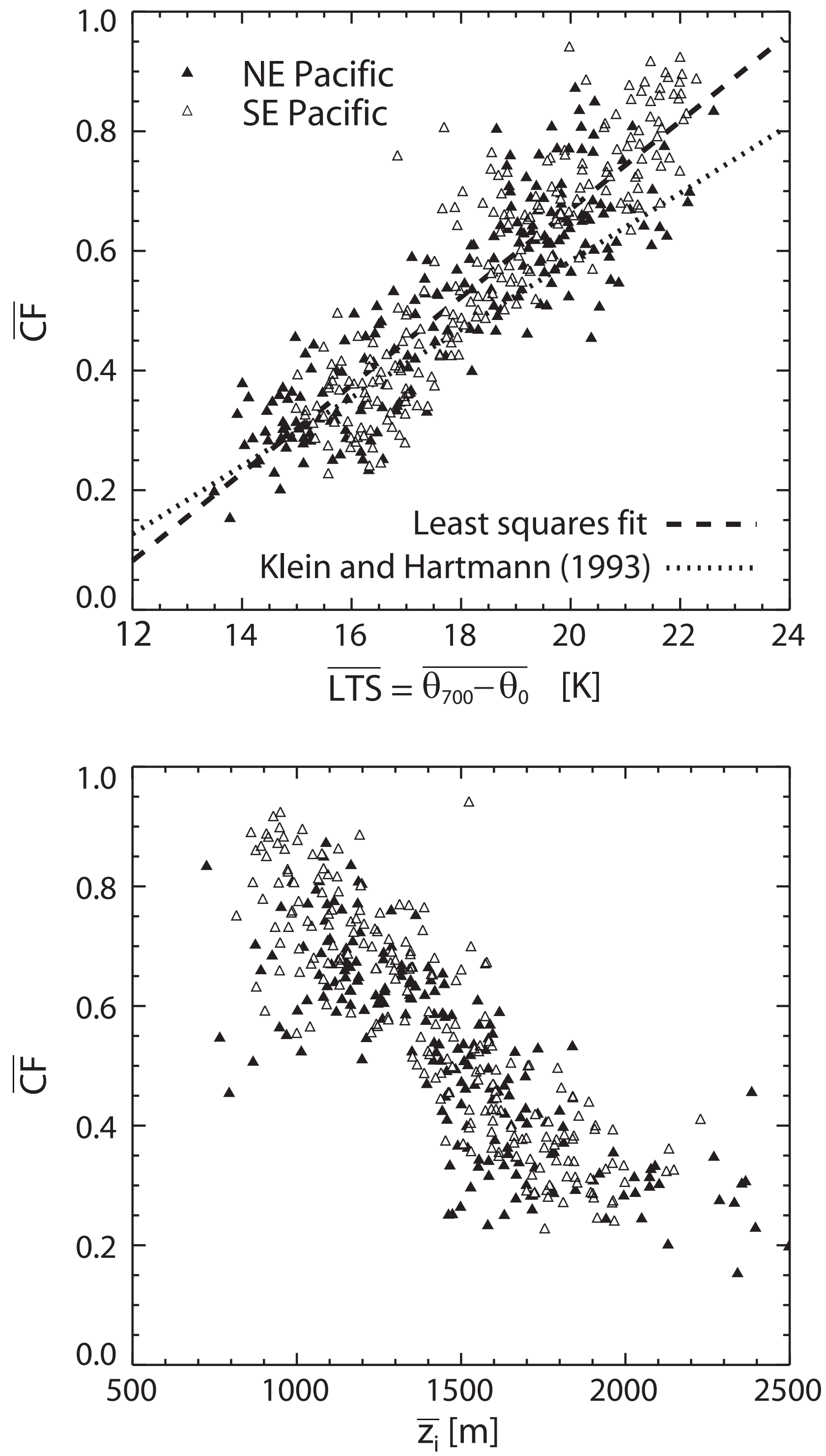
NE Pacific
SE Pacific
Least squares fit
Klein and Hartmann (1993)
$\overline{CF}$
$\overline{LTS} = \overline{\theta_{700} - \theta_0}$ [K]
$\overline{z}_i$ [m]

Figure 18: